Ice clouds as nonlinear oscillators

Cite as: Chaos 36, 043115 (2026); doi: 10.1063/5.0297531
Submitted: 20 August 2025 · Accepted: 13 March 2026 ·
Published Online: 9 April 2026

View Online Export Citation CrossMark

Hannah Bergner and Peter Spichtinger[a)]

AFFILIATIONS

Institute for Atmospheric Physics, Johannes Gutenberg University, Mainz, Germany

[a)]**Author to whom correspondence should be addressed:** spichtin@uni-mainz.de

ABSTRACT

Clouds are important features of the atmosphere, determining the energy budget by interacting with incoming solar radiation and outgoing thermal radiation, respectively. For pure ice clouds, the net impact of the radiative effect is still unknown. In this study, we develop a simple but physically consistent ice cloud model and analyze it using methods from the theory of dynamical systems. We find that the model constitutes a nonlinear oscillator with two Hopf bifurcations in the relevant parameter regime. In addition to the characterization of the equilibrium states and the occurring limit cycle, we find scaling behaviors of the bifurcations and the limit cycle, reducing the parameter space crucially. Finally, the model shows very good agreement with real measurements, indicating that the main physics is captured and such simple models are helpful tools for investigating ice clouds.

Investigations of clouds need well-characterized models for simulating relevant properties as well as helping to interpret measurements. Here, we propose a simple but robust model for ice clouds, which is characterized using the theory of dynamical systems, and compare to real measurements. The proposed model is not the end of the line but rather a first step in systematic deriving of consistent models of different complexities.

I. INTRODUCTION

Clouds are frequently found to be distributed over the whole globe. A portion of about 60%–70% of the Earth is permanently covered by clouds,[1] which are also distributed over several vertical levels in the troposphere (i.e., up to 12–15 km altitude). Clouds are composed of myriads of water particles of different phases. For low vertical levels in the atmosphere, i.e., at temperatures above the triple point ($T_t = 273.16$ K), clouds contain only liquid water droplets. For the temperature range between the triple point and about $T \sim 235$ K, liquid water can still exist, however, the solid phase, i.e., classical hexagonal ice, is the stable phase. At temperatures around $T \sim 235$ K, liquid water freezes spontaneously and below this temperatures, pure liquid water cannot exist anymore,[2] thus clouds at these temperatures (i.e., at high altitudes close to the tropopause) are completely composed of ice crystals.

Clouds play a major role for the Earth–Atmosphere system. They determine the hydrological cycle by producing precipitation and also drive atmospheric flows by the huge amount of energy, which is released at phase transitions.[3] Vigorous systems like thunderstorms are only possible because of this anomaly of water. Finally, clouds also regulate the energy budget of the system itself, controlling the impact of radiation. Clouds interact with incoming solar radiation by scattering and partly reflecting solar radiation; in the presence of clouds, less solar energy is transported into the system as compared to the clear sky case, leading to a cooling effect (albedo effect). On the other hand, they partly absorb and re-emit thermal radiation as radiated by the Earth's surface (as an almost perfect black body), thus keeping more energy in the system as compared to the clear sky case (greenhouse effect). The difference of these two effects leads to the net climate effect of clouds. For low level liquid clouds, the albedo effect is dominant, hence leading to a net cooling of these clouds. For clouds at higher altitudes, i.e., clouds containing ice particles, the net effect is still uncertain; for pure ice clouds, we do not even know the sign of the net effect. This results also from the fact that for ice clouds both effects (cooling vs warming) are of comparable values but with different signs. Thus, small variations in microphysical properties as, e.g., the size of particles lead to significant changes in the net effect, as demonstrated by Zhang *et al.*[4] For high level ice clouds, often a net warming is assumed,[5] but recent estimations indicate different or even inconclusive outcomes.[6] Since for clouds, thermodynamics decides about the mass concentration in first order, the number concentration of ice particles can be directly translated into the size of particles and thus into the radiation calculations; this is crucial since smaller particles scatter more efficiently than larger ones.[7]

In general, the number concentration of ice particles is determined by the generation mechanisms, i.e., the nucleation pathway. In recent studies,[8,9] a distinction between generally different formation pathways was formulated, termed as *liquid origin* cirrus and *in situ* cirrus, respectively. The former pathway is characterized by pre-existing liquid cloud droplets at states close to thermodynamic equilibrium (saturation over water), which freeze to ice particles, either triggered by solid aerosols or spontaneously. This pathway is only valid in the temperature range $T > 235$ K, where liquid water can still exist. The latter pathway takes place at low temperature; water vapor is either directly deposited as ice on solid aerosol particles (so-called heterogeneous nucleation) or supercooled aqueous solution droplets freeze spontaneously. The nucleation mechanisms might have a big impact on the resulting number concentration from such a freezing/nucleation event. The resulting number concentration might be limited either by the amount of available ice nucleating particles (particle limited regime) or even by the available water vapor for producing cloud or solution droplets (supersaturation limited regime). The latter one is crucially depending on local dynamics, which leads to a source of supersaturation by adiabatic cooling in upward motions.

In addition to the details of nucleation processes, which are barely understood on a molecular level, many other processes in clouds are quite uncertain. Very often, we find that the processes might be understood to some extend on a particle level, but the scaling up to the ensemble is not clear. This points to the fact that in contrast to fluid dynamics where a general and well accepted theory is available (i.e., Navier–Stokes equations or approximations of it), this is not the case for clouds. Actually, there is **no** generally accepted theory of clouds in terms of a closed system of partial differential equations or something similar. Processes are mostly known on particle basis and reaction rates are formulated often in an ad hoc manner in order to take into account the needs for the respective applications.

There are only few attempts to formulate a general theory of clouds for some parts of the phase space of clouds, mostly in the field of liquid clouds. For ice clouds, we are aware of some attempts of deriving a Boltzmann-type evolution equation.[10] However, none of them resulted into an overall and generally accepted cloud formulation. For a review of such formulations, see Khain *et al.*[11]

In this study, we focus on pure ice clouds in a low temperature regime ($T < 240$ K), where *in situ* formation takes place at levels in the upper troposphere. For the formation of ice particles in this regime, environmental conditions far away from thermodynamic equilibrium (i.e., saturation with respect to ice) are required; even after the formation process, ice clouds remain in a state out of equilibrium because relaxation toward equilibrium can be quite slow. Thus, ice clouds form a non-equilibrium multiphase system. Ice clouds are also multiscale phenomena, showing structure formation and emergence of pattern, thus not only relevant in terms of microscale processes but also in the propagation of information through all scales. For investigation of such phenomena simple but consistent models are necessary, which contain the main features of the physics, but are simple enough for coupling to fluid dynamics equations. For instance, if we want to investigate issues such as predictability, we have to make sure that the cloud model as coupled to the equations of motion in terms of reaction rates is well-posed. Otherwise, investigations about representing clouds on different scales in numerical models with changing grid resolutions remain a bit arbitrary.

In this study, we derive a simple ice cloud model on the basis of a consistent formulation of cloud processes. Here, we include the most important processes, such as ice nucleation, growth, and evaporation by water vapor diffusion and sedimentation of ice crystals, respectively. After some simplifications, we end up with a three-dimensional (3D) system of nonlinear autonomous ordinary differential equations, which then can be analyzed by the theory of dynamical systems. There were several former studies, investigating cloud models as dynamical systems, e.g., for liquid and mixed-phase clouds,[12–15] but also for aerosol–cloud systems.[16,17] Our investigation is based on the former study by Spreitzer *et al.*,[18] which evaluated a small part of the phase space of ice clouds, i.e., so-called subvisible cirrus clouds at low vertical updrafts; they used a slightly different model, which could not be analyzed in detail. Our approach extends this former study and aims to derive a much more detailed analysis; since our current model is "much simpler," however still realistic, we can determine several properties in an analytical or semi-analytical way, including also the regime of subvisible cirrus.[18] We determine equilibrium states and their quality using linearization approaches. In addition, we determine bifurcations and, thus, periods of limit cycles with numerical evaluations. Finally, the model is compared to real measurements in order to determine its feasibility for the use in extended models.

The study is structured as follows. In Sec. II, we present an overview of the ice cloud model including the approach, setting, main assumptions, and the equations constituting the 3D nonlinear system of ordinary differential equations for the ice cloud model. In Sec. III, we then discuss the physical variables and processes for modeling ice clouds in the low temperature regime in detail and derive the explicit model equations which were already presented in Sec. II. The system is then characterized and analyzed in terms of dynamical systems theory in Sec. IV, i.e., we determine equilibrium states, their quality, and possible limit cycles and additionally investigate scaling properties of the system. While the equilibrium states and their quality are determined by explicit calculations and mathematical arguments, the study of the limit cycles and investigation of the scaling properties are carried out using numerical analysis. In Sec. V, we compare the model results with real measurements. Finally, we summarize the work, draw some conclusions, and present an outlook for future work.

II. OVERVIEW OF THE MODEL

In this section, we give an overview over the ice cloud model and present the approach, setting, main assumptions, and equations. The details of the relevant physics, the model derivation, and in-depth presentation of the individual terms of the equations are given in Sec. III.

A. Approach

The ice cloud model is supposed to describe the time evolution of the key microphysical properties of the part of an ice cloud

contained inside a fixed parcel or box of air (which is followed in a Lagrangian manner).

Moreover, we take a bulk model ansatz: A cloud usually consists of a vast number of water particles and it is impossible to model the evolution of the properties of all those particles individually. One common ansatz for modeling the cloud properties is to take a probability distribution for the masses of the cloud particles and formulate equations for the evolution of the distribution in space and time. From this, one can furthermore derive equations for the general moments μ_k of the distribution. For this purpose, we assume that our considered volume (i.e., the box) is well-mixed, so the cloud can be characterized by averaged quantities, formally represented by the general moments of the distribution. This assumption is key for the derivation of a bulk model. To simplify further, we restrict ourselves to a 2-moment scheme as the basis for the ice cloud model and thus only consider the k-moments for $k = 0, 1$. The 0-moment gives the ice crystal number concentration $\mu_0 = n$, while the 1-moment is the ice crystal mass concentration $\mu_1 = q$; both quantities can be interpreted as mean values of the homogeneous mixture of cloud particles in the box. For more details, see Sec. III D and Appendix A.

B. Setting and general assumptions

We focus on a low temperature regime $T < 240\,\mathrm{K}$ with pure ice clouds and where *in situ* formation of ice crystals takes place (see Secs. III A and III B) and want to model the microphysical properties of the portion of an ice cloud inside an air parcel moving upward with a fixed vertical velocity w.

For the ice cloud model, we only consider the *in situ* formation of ice crystals in the low temperature regime, where ice crystals "directly" form from water vapor (without any transition through the liquid water phase) and among the different possible *in situ* formation pathways we only consider homogeneous nucleation, i.e., the freezing of aqueous solution droplets (see Sec. III B).

Since ice crystals do appear in a huge variety of shapes that cannot be realistically represented in a simple model, an approximation thereof has to be chosen. For our model, we thus assume the ice crystals to be spherical, which is further motivated and elaborated in Sec. III C.

For the above (in Sec. II A) mentioned probability distribution for the masses of ice crystals in the low temperature regime, we make the assumption that it is a fixed type of distribution and assume that it is lognormal (see Sec. III D).

Apart from the variables of ice crystal number concentration n and ice crystal mass concentration q given by the 2-moment scheme approach (as described in Sec. II A), we consider another variable for the ice cloud model, namely, the saturation ration $s = S_i$ of water vapor over ice [see Sec. III B, especially Eq. (20)]. The ice cloud model will give equations for the time evolution of these three variables: n, q (from the 2-moment scheme approach) and s (as a variable for the humidity).

C. Relevant processes and basic structure of the model system

We now present the relevant processes for the ice cloud model and the resulting general structure of system. The variables we want to model are the ice crystal number concentration n, the ice crystal mass concentration q, and the saturation ratio s of water vapor over ice.

We consider the following physical processes that contribute to the change rates of the variables n, q, s (for more details see Secs. III B and III E):

- **Nucleation:** The nucleation of new ice particles impacts the values of all three variables n, q, and s. As already mentioned above, we only consider homogeneous freezing for our model, i.e., the freezing of aqueous solution droplets (see Sec. III B). While the number and mass concentrations n and q increase when new ice crystals arise from nucleation, the saturation ratio s decreases since the water content of the newly nucleated ice crystals is taken from the water vapor of the ambient air. The contribution to the change rates of n, q, and s due to nucleation are denoted by $\mathbf{Nuc}_n$, $\mathbf{Nuc}_q$, and $\mathbf{Nuc}_s$ respectively.
- **Sedimentation:** We have to consider the effect of sedimentation on n and q and introduce the sedimentation terms $\mathbf{Sed}_n$ and $\mathbf{Sed}_q$ for the contributions to the changes rates of n and q due to sedimentation. For the sedimentation terms, we will use an approximation over the vertical extend of the considered box in order to avoid a vertical transport equation, i.e., a system of partial differential equations [see Eq. (60)]. This approximation also includes the choice of a sedimentation parameter F with $0 < F \leq 1$ representing the strength of the sedimentation from above into the considered box in relation to the sedimentation out of the box.
- **Deposition/evaporation:** Growth and evaporation impact the ice crystal number and mass concentrations. They act in different ways on the variables n and q. For a supersaturated regime ($s > 1$), the ice particles can grow by diffusion while the number concentration is not affected by growth. For evaporation, both mass and number concentrations are depleted. We denote the contribution to the change rate of the mass concentration due to diffusional (de-)growth by $\mathbf{Dep}_q$ (molecules are deposited on the particle's surface) and the contribution to the change rate of the number concentration due to evaporation by $\mathbf{Evap}_n$ (where $\mathrm{Evap}_n = 0$ for $s > 1$). In this article we mainly focus on a supersaturated regime, i.e., the case where $s > 1$, and only mention an ansatz for the evaporation term Evap_n for completeness.
  Since the change of the mass concentration due to diffusional (de-)growth is by transfer of water vapor from the ambient air, it also induces a corresponding change in the saturation ratio, which we denote by $\mathbf{Dep}_s$.
- **Cooling:** For our model setup, we assume a constant vertical velocity w. This leads to adiabatic changes in temperature and pressure, which consequently affect our thermodynamic control variable, the saturation ratio s of water vapor over ice. In Sec. III B, we explain that the resulting effect on the saturation ratio can be formulated in terms of a cooling term **Cool** which only depends on the vertical velocity w and not explicitly on the change rates of temperature and pressure. Moreover, we illustrate in Sec. III B that it is a reasonable assumption in our setting to assume that change rates of temperature and pressure only (implicitly) appear in the evolution equation for s, while the evolution equations for temperature and pressure themselves are skipped, i.e., we assume temperature and pressure to remain constant.

Effects due to the collision of particles are neglected in our model since the sticking efficiency in very low in the cold temperature regime (see Sec. III E 5).

The **basic structure of the ice cloud model** is then as follows:

$$\frac{\mathrm{d}n}{\mathrm{d}t} = \mathrm{Nuc}_n, +\mathrm{Evap}_n + \mathrm{Sed}_n, \tag{1}$$

$$\frac{\mathrm{d}q}{\mathrm{d}t} = \mathrm{Nuc}_q + \mathrm{Dep}_q + \mathrm{Sed}_q, \tag{2}$$

$$\frac{\mathrm{d}s}{\mathrm{d}t} = \mathrm{Cool} + \mathrm{Nuc}_s + \mathrm{Dep}_s, \tag{3}$$

with total derivatives $\frac{\mathrm{d}\psi}{\mathrm{d}t}$ for a variable ψ. Later, it is shown that this is an autonomous nonlinear ordinary differential equation (ODE) system.

D. The equations for the ice cloud model

Here, we briefly present the full equations for the ice cloud model for an overview and state where in the following sections the derivations of the individual terms can be found.

The ice cloud model turns out to be 3D system of ODEs with ice crystal number concentration n, ice crystal mass concentration q, and saturation ratio over ice s as variables. Its full equations are

$$\frac{\mathrm{d}n}{\mathrm{d}t} = A_n \exp(p_{1\mathrm{e}}(s-p_2)) + B_q n^{\frac{5}{3}} q^{-\frac{2}{3}}(s-1)H(1-s) - FC_n n^{\frac{1}{3}} q^{\frac{2}{3}}, \tag{4}$$

$$\frac{\mathrm{d}q}{\mathrm{d}t} = A_q \exp(p_{1\mathrm{e}}(s-p_2)) + B_q n^{\frac{2}{3}} q^{\frac{1}{3}}(s-1) - FC_q n^{-\frac{2}{3}} q^{\frac{5}{3}}, \tag{5}$$

$$\frac{\mathrm{d}s}{\mathrm{d}t} = Dws - A_s \exp(p_{1\mathrm{e}}(s-p_2)) - B_s n^{\frac{2}{3}} q^{\frac{1}{3}}(s-1). \tag{6}$$

This is a nonlinear autonomous ODE system, depending on the environmental parameters pressure p, temperature T, vertical velocity w, and a sedimentation parameter F. The ranges for the parameters are given in Table I, which are representative for the environmental conditions in the upper troposphere.

The individual terms of the ODE system are as follows:

- The nucleation terms are

$$\mathrm{Nuc}_n = A_n \exp(p_{1\mathrm{e}}(s-p_2)), \tag{7}$$

TABLE I. Ranges of relevant parameters for the 3D ice cloud model, Eqs. (4)–(6).

Parameter	Dimension	Range
Pressure p	hPa	$200 \le p \le 300$
Temperature T	K	$190 \le T \le 240$
Vertical velocity w	m/s	$0.0005 \le w \le 2$
Sedimentation parameter F	1	$0.01 \le F \le 1$

$$\mathrm{Nuq}_q = A_q \exp(p_{1\mathrm{e}}(s-p_2)), \tag{8}$$

$$\mathrm{Nuc}_s = -A_s \exp(p_{1\mathrm{e}}(s-p_2)), \tag{9}$$

as given in Eqs. (43)–(45), where A_n and A_q depend on temperature T and pressure p, the terms $p_{1\mathrm{e}}$ and p_2 depend on temperature T [see Eqs. (A18)–(A19)], and $A_s = A_q \frac{p}{\varepsilon p_{\mathrm{si}}}$ as in Eq. (45).

- The deposition term representing the effect on the mass concentration q due to diffusional (de-)growth is

$$\mathrm{Dep}_q = B_q n^{\frac{2}{3}} q^{\frac{1}{3}}(s-1), \tag{10}$$

as given in Eq. (51) and derived in Appendix A 4. The factor B_q depends on temperature and pressure and is given in Eq. (52).

The deposition term for the effect on the saturation ratio is given by

$$\mathrm{Dep}_s = -B_s n^{\frac{2}{3}} q^{\frac{1}{3}}(s-1), \tag{11}$$

as in Eq. (53) and where $B_s = B_q \frac{p}{\varepsilon p_{\mathrm{si}}}$ depends on pressure and temperature [see also Eq. (53)].

- As already mentioned above, we concentrate on the supersaturated regime with $s > 1$ in this article. For completeness, however, we want to mention the possible choice for the evaporation term for the nucleation by the ad hoc ansatz $\mathrm{Evap}_n = \frac{n}{q}\mathrm{Dep}_q H(1-s)$ as given Eq. (54) which results in

$$\mathrm{Evap}_n = B_q n^{\frac{5}{3}} q^{-\frac{2}{3}}(s-1)H(1-s), \tag{12}$$

where H denotes the Heaviside function, such that $\mathrm{Evap}_n = 0$ if $s > 1$ as supposed in the supersaturated regime, and where B_q is the same as in the deposition term Dep_q.

- The sedimentation terms are

$$\mathrm{Sed}_n = -FC_n n^{\frac{1}{3}} q^{\frac{2}{3}}, \tag{13}$$

$$\mathrm{Sed}_q = -FC_q n^{-\frac{2}{3}} q^{\frac{5}{3}}, \tag{14}$$

as given in Eqs. (69)–(70), where F is a sedimentation parameter as introduced in Sec. III E 4 and C_n and C_q depend on temperature and pressure as well as the vertical extension Δz of the considered box [see Eq. (66)]. The linear dependence of the sedimentation terms on F is directly formulated in this way.

- The cooling term representing the effect of the vertical velocity w on the saturation ratio is given by

$$\mathrm{Cool} = Dw\,s = \underbrace{\left[\frac{L}{c_p R_v T^2} - \frac{1}{R_d T}\right] g}_{=:D}\, ws, \tag{15}$$

as given in Eq. (30), where D depends on temperature; the linear dependence of the term Cool is indicated directly in this formulation. Furthermore, note that the cooling term is the only term on the right-hand side of the ODE system that explicitly depends on w.

Using the notation $x = (n, q, s)^T$ we could write the system with a suitable 3D vector field V as an autonomous ODE system $\dot{x} = V(x)$. Note, that this system is not well-defined for initial conditions without a cloud, i.e., for $x_0 = (0, 0, s_0)$; the terms on the

right-hand side include singularities of the form $n^{-\alpha}$ or $q^{-\beta}$ (with $\alpha, \beta > 0$). For the supersaturation regime ($s > 1$), a regularization of the sedimentation term

$$-FC_q n^{-\frac{2}{3}} q^{\frac{5}{3}} \approx -FC_q (n + n_{\text{small}})^{-\frac{2}{3}} q^{\frac{5}{3}} \tag{16}$$

might be applied. Nevertheless, even if the singularities are removed, the right-hand side is not Lipschitz continuous for initial values $n = 0$ or $q = 0$ because of terms $n^\alpha q^\beta$ with $0 \le \alpha < 1, 0 \le \beta < 1$. Thus, for initial value problems starting at such states the standard theory[19] (p. 68) cannot be applied. For other starting points, existence and uniqueness of solutions is guaranteed, since the right-hand side is smooth; this is also true for the system without a regularization. We want to note here, that even for the initial values $n = 0$ or $q = 0$, uniqueness might be obtained, following the arguments by Hanke and Porz[20] to produce a mathematically unique solution with additional physical conditions. This will be subject of future investigations. However, for our investigations in the present study these details might be not relevant, since we are mainly interested in the long time behavior, i.e., the qualitative properties of the system; then we can assume that n, q are positive.

III. PHYSICAL VARIABLES AND PROCESSES AND DERIVATION OF THE MODEL EQUATIONS

In this section, we define the general setting for the model. We give a general description of clouds as an ensemble of many particles, embedded into atmospheric flows. Nevertheless, later we simplify the whole system to a 3D dynamical system, describing Lagrangian air parcels transported by prescribed air motion.

At the end of this section, the explicit equations for the individual terms of the ice cloud model are derived in Sec. III E. In Sec. IV, the model system is analyzed, and in Sec. V, some comparison with measurements are carried out.

A. Thermodynamic environment

For modeling ice clouds, we have to set up the thermodynamic environment. We consider air and water vapor in a control volume V (box or parcel) as ideal gases as described by the ideal gas law,

$$p_k V = M_k R_k T \Leftrightarrow p_k = \rho_k R_k T, \quad \text{with } \rho_k = \frac{M_k}{V}, \tag{17}$$

using the partial pressure p_k, the specific gas constant $R_k = \frac{R^*}{M_{\text{mol},k}}$ as derived from the universal gas constant $R^* = 8.314\,462\,\text{J mol}^{-1}\,\text{K}^{-1}$, and the temperature T. The partial masses of the gases are denoted by M_k. The index d indicates dry air, the index v denotes water vapor. The total pressure in the volume is determined by Dalton's law, i.e., $p = p_d + p_v$; however, a good approximation is given by $p \approx p_d$ (since $p_d \gg p_v$). The parcel can be seen as one vertical layer at a certain height within a full atmospheric column. The pressure is determined by the hydrostatic balance, i.e., the air mass in the vertical column

$$\frac{\partial p}{\partial z} = -g\rho. \tag{18}$$

We consider the low temperature regime in the upper troposphere, i.e., temperatures in the range $190 \le T \le 240\,\text{K}$. The corresponding air pressure values are considered to be within the range $200 \le p \le 300\,\text{hPa}$. In addition to water vapor, we also consider the mass of the condensed water phase, i.e., the total mass of ice particles M_i. At these low temperatures, liquid water does not exist in the atmosphere,[2] thus we can restrict the system to gaseous and solid phases of water. For the further investigations, we use the mass concentration of water vapor $q_v = \frac{M_v}{M_d}$ and the mass concentration of ice $q_i = \frac{M_i}{M_d}$. In fact, the total mass $M = M_d + M_v + M_i$ can be approximated by the mass of air since the relative contribution of water substances is less than 10^{-3}, thus $M \approx M_d$.

B. Phase changes and saturation ratio

We are only interested in the formation of ice crystals within the respective low temperature region, i.e., the formation of ice "directly" from water vapor without any transition through the liquid phase. Recently, formation pathways of this type were grouped together and named "*in situ* formation."[8,9] From these different pathways, we only consider the pathway of homogeneous freezing of aqueous solution droplets.[21,22] At these atmospheric conditions, hexagonal ice (I_h) is the stable solid phase of water.[2] For assuming water vapor as an ideal gas, the thermodynamic equilibrium of these water phases is approximately determined by the Clausius–Clapeyron equation[23]

$$\frac{\mathrm{d}p_{\text{si}}}{\mathrm{d}T} = \frac{L p_{\text{si}}}{R_v T^2}, \tag{19}$$

using the specific latent heat of sublimation L, which is slightly dependent on temperature;[24] p_{si} denotes the saturation vapor pressure over hexagonal ice (see also Appendix A 3). The thermodynamical control variable for determining ice cloud processes is the saturation ratio over ice,

$$S_i := \frac{p_v}{p_{\text{si}}(T)} = \frac{p q_v}{\varepsilon p_{\text{si}}(T)}, \tag{20}$$

using the water vapor mixing ratio q_v, and the ratio of molar masses of water and air $\varepsilon = \frac{M_{\text{mol},v}}{M_{\text{mol},d}} \approx 0.622$.

We often consider changes in the saturation ratio, which are governed by changes in temperature, pressure, and specific humidity, respectively. For this purpose, we investigate the total derivative of the saturation ratio, as given by

$$\frac{\mathrm{d}S_i}{\mathrm{d}t} = \frac{\partial S_i}{\partial T}\frac{\mathrm{d}T}{\mathrm{d}t} + \frac{\partial S_i}{\partial p}\frac{\mathrm{d}p}{\mathrm{d}t} + \frac{\partial S_i}{\partial q_v}\frac{\mathrm{d}q_v}{\mathrm{d}t}, \tag{21}$$

using the partial derivatives

$$\frac{\partial S_i}{\partial T} = -S_i \frac{L}{R_v T^2}, \quad \frac{\partial S_i}{\partial p} = \frac{S_i}{p}, \quad \frac{\partial S_i}{\partial q_v} = \frac{S_i}{q_v} = \frac{p}{\varepsilon p_{\text{si}}}, \tag{22}$$

where we have used the Clausius–Clapeyron equation (19).

We can split the changes in temperature into adiabatic and diabatic components, i.e., temperature changes driven by adiabatic expansion due to vertical upward motions and temperature changes induced by latent heat release during phase changes. These

temperature rates can be represented as follows:

$$\left.\frac{\mathrm{d}T}{\mathrm{d}t}\right|_{\text{adiabatic}} = \frac{\mathrm{d}T}{\mathrm{d}z}\frac{\mathrm{d}z}{\mathrm{d}t} = -\frac{g}{c_p}w, \tag{23}$$

$$\left.\frac{\mathrm{d}T}{\mathrm{d}t}\right|_{\text{diabatic}} = -\frac{L}{c_p}\frac{\mathrm{d}q_v}{\mathrm{d}t}. \tag{24}$$

Note that we omit other diabatic processes, as, e.g., friction or radiation processes. Using these expressions, we can determine the change in S_i due to temperature changes

$$\begin{aligned}\frac{\partial S_i}{\partial T}\frac{\mathrm{d}T}{\mathrm{d}t} &= -S_i\frac{L}{R_vT^2}\left(\left.\frac{\mathrm{d}T}{\mathrm{d}t}\right|_{\text{adiabatic}} + \left.\frac{\mathrm{d}T}{\mathrm{d}t}\right|_{\text{diabatic}}\right)\\ &= \frac{Lg}{c_pR_vT^2}S_iw + \frac{L^2}{c_pR_vT^2}S_i\frac{\mathrm{d}q_v}{\mathrm{d}t}.\end{aligned} \tag{25}$$

The adiabatic pressure change, assuming hydrostatic balance,

$$\frac{\mathrm{d}p}{\mathrm{d}t} = \frac{\mathrm{d}p}{\mathrm{d}z}\frac{\mathrm{d}z}{\mathrm{d}t} = -g\rho w \tag{26}$$

also influences the saturation ratio, thus

$$\frac{\partial S_i}{\partial p}\frac{\mathrm{d}p}{\mathrm{d}t} = -\frac{S_i}{p}g\rho w = -S_i\frac{g}{R_dT}w \tag{27}$$

and changes in the water vapor concentration q_v, finally, give the rate

$$\frac{\partial S_i}{\partial q_v}\frac{\mathrm{d}q_v}{\mathrm{d}t} = \frac{p}{\varepsilon p_{\text{si}}}\frac{\mathrm{d}q_v}{\mathrm{d}t}. \tag{28}$$

Putting all rates together and sorting leads to the final rate for the saturation over ice,

$$\frac{\mathrm{d}S_i}{\mathrm{d}t} = \left[\frac{L}{c_pR_vT^2} - \frac{1}{R_dT}\right]gwS_i + \left[\frac{L^2}{c_pR_vT^2}S_i + \frac{p}{\varepsilon p_{\text{si}}}\right]\dot{q}_v. \tag{29}$$

In the cold temperature regime, the total amount of water vapor is very small, thus the impact of latent heat release, as represented by the first term in the second bracket, can be neglected by a good approximation. Actually, for temperatures lower than $T \sim 230\,\text{K}$, the contribution of this term is less than 10% (with a maximum of ∼20% at $T \sim 240\,\text{K}$ and constitute contributions of less than 1% below $T \sim 210\,\text{K}$). Therefore, we use the following expression:

$$\begin{aligned}\frac{\mathrm{d}S_i}{\mathrm{d}t} &= \left[\frac{L}{c_pR_vT^2} - \frac{1}{R_dT}\right]gwS_i + \left[\frac{L^2}{c_pR_vT^2}S_i + \frac{p}{\varepsilon p_{\text{si}}}\right]\dot{q}_v\\ &\approx \underbrace{\left[\frac{L}{c_pR_vT^2} - \frac{1}{R_dT}\right]gwS_i}_{\text{Cool}} + \left[\frac{p}{\varepsilon p_{\text{si}}}\right]\dot{q}_v\\ &= \underbrace{Dw\,S_i}_{\text{Cool}} + \frac{p}{\varepsilon p_{\text{si}}}\dot{q}_v,\end{aligned} \tag{30}$$

introducing the term Cool governing the component of the time evolution of the saturation ratio due to the vertical velocity w. This term together with the second term $\frac{p}{\varepsilon p_{\text{si}}}\dot{q}_v$, describing phase changes, will also appear in the complete model. We will later use the notation $s := S_i$. Note that the first term in Eq. (30) constitutes a source for supersaturation in the case of a positive vertical velocity $w > 0$, i.e., if there is an upward motion. The coefficient D depends on temperature T, and the linear dependence of Cool on the vertical velocity w is directly indicated.

For analytical investigations, i.e., for the derivation of equilibrium states (equilibrium points or manifolds, as, e.g., limit cycles), we formally investigate the system for $t \to \infty$, since the equilibria are only asymptotically reached from initial conditions different from these states. Physically, this is not possible and also not meaningful, since we cannot cool the system arbitrarily long. Thus, we follow the approach of former investigations, in terms of "freezing" the environmental conditions to constant values of temperature and pressure, considering the impact of vertical upward motion in the rates of s only. This general approach of "constant environmental states" was successfully applied in studies on processes in warm and mixed-phase clouds[12–15,25] and also in our former investigation of subvisible cirrus clouds.[18] Actually, this does not mean that our investigation is only valid for arbitrary long time evolution; the system is characterized for certain environmental conditions, which provides information about the general properties. This might be useful for practical applications, as we will see later in Sec. V, where we compare the system with real measurements.

C. General assumptions for ice crystals

Ice crystals usually have quite irregular shapes with inherent hexagonal structures due to the stable solid phase (hexagonal ice I_h). The exact and detailed shape and its evolution in time depend crucially on the environmental conditions.[26]

Since there is a huge variety of shapes for ice crystals[27,28] and we cannot represent this variability within a simple model, we have to choose an approximation. There are two different reasons for choosing a spherical shape for ice crystals in our model. First, we are interested in the low temperature regime; thus, the available amount of water vapor is limited, so ice crystals stay quite small and are almost spherical; from measurements, we know that the maximum radius should not exceed values of $100\,\mu\text{m}$.[6] The complex shapes of ice crystal usually appear for the warm temperature regime (i.e., $T > 240\,\text{K}$) together with much larger sizes. Second, from theoretical and computational investigations[29] we know that in a certain distance to a non-spherical crystal, the resulting water vapor field is almost the same as for a larger spherical ice crystal. Thus, we use a spherical shape for ice crystals, with the common relationship between mass and radius,

$$m = \frac{4}{3}\pi\rho_b r^3 \;\Leftrightarrow\; r = \sqrt[3]{\frac{3}{4\pi\rho_b}}m^{\frac{1}{3}} = cm^{\frac{1}{3}} \tag{31}$$

with $\rho_b = 810\,\text{kg}\,\text{m}^{-3}$ as the bulk density of ice.[30] The radius will appear later in the growth equation, when we specify a spherical shape.

D. General assumptions for cloud ensembles

Clouds are usually composed by myriads of water particles, thus we have to consider a cloud as a statistical ensemble. As described by Spreitzer *et al.*,[18] a generic way for describing the cloud

ensemble would be to use a probability distribution $f(m, x, t)$ for the masses of cloud particles and investigate the evolution of the distribution in time and space. This would lead to a Boltzmann-type evolution equation for the distribution, i.e.,

$$\frac{\partial(\rho f)}{\partial t} + \nabla_x \cdot (\rho f u) + \frac{\partial(\rho f g)}{\partial m} = \rho h, \tag{32}$$

with transport with velocity u, growth with a rate function g, and other sources and sinks, described by h. From this equation, we can derive (infinitely many) equations for the general moments

$$\mu_k[m] := \int_0^\infty m^k f(m, x, t)\, \mathrm{d}m, \quad k \in \mathbb{N}_0 \tag{33}$$

of the distribution if the integral converges. The general formulation of moment equations as derived from the Boltzmann-type approach is presented in Appendix A.

Since we can neither solve infinitely many equations nor do we have a general and consistent description of the sources and sink term h on the right-hand side, we make the following assumptions for simplification,

- We only use two equations, i.e., for the moments $k = 0, 1$ and use a closure condition. Usually, the distribution is normalized by the cloud particle number concentration n, thus we obtain equations for the number concentration $\mu_0 = n$ and the mass concentration $\mu_1 = q$. For ice crystals in the low temperature regime ($T < 240\,\mathrm{K}$), we assume a fixed type of distribution, i.e., a lognormal distribution,

$$f(m) = \frac{n}{\sqrt{2\pi}\log(\sigma_m) m} \exp\left(-\frac{1}{2}\left(\frac{\log\left(\frac{m}{m_m}\right)}{\log(\sigma_m)}\right)^2\right), \tag{34}$$

  with the modal mass m_m and the geometric standard deviation σ_m. Thus, the general moments can be calculated analytically as

$$\mu_k[m] = n m_m^k \exp\left(\frac{1}{2}\left(k \log \sigma_m\right)^2\right). \tag{35}$$

  The closure is determined by a fixed ratio of moments r_0, i.e.,

$$r_0 = \frac{\mu_2 \mu_0}{\mu_1^2} = \exp\left(\left(\log(\sigma_m)\right)^2\right), \tag{36}$$

  which can be used for calculating the moments

$$\mu_k[m] = n m_m^k r_0^{\frac{k^2}{2}} = n \bar{m}^k r_0^{\frac{k(k-1)}{2}}, \tag{37}$$

  with the mean mass $\bar{m} := \frac{q}{n}$. We set $r_0 = \text{const.}$ and thus the geometric standard deviation σ_m is constant; as in former investigations,[31] we set $r_0 = 3$. The choice of a lognormal distribution is motivated by the shape of measured size distributions,[32] although other (analytical) types of distributions might be used as well.
- For the right-hand side, i.e., the formation and annihilation processes of ice particles, we will use meaningful parameterizations, which are partly derived from the moment approach (see also Appendix A).

Thus, we will formulate our model using the mean variables number concentration of ice particles $n = \mu_0$ and mass concentration of ice particles $q = \mu_1$.

E. Relevant processes and derivation of the model equations

In the following, we discuss the relevant processes for the ice cloud model in more detail and derive the explicit equations for the terms related to the considered processes.

1. Effect of the vertical updraft

As already discussed in Sec. III B, the constant vertical velocity w we assume leads to adiabatic changes in pressure and temperature whose influences on the change rate of the saturation ratio s can be collected in a "cooling term." This term takes the form

$$\mathrm{Cool} = D w s, \tag{38}$$

as derived in Eq. (30), where $D = \left[\frac{L}{c_p R_v T^2} - \frac{1}{R_d T}\right] g$ depends on the temperature T and the vertical velocity w is a linear contribution.

2. Particle formation—Ice nucleation

For ice formation at low temperatures, two nucleation processes might be relevant, i.e., (1) homogeneous freezing of aqueous solution droplets[21] and (2) heterogeneous nucleation at solid aerosol particles. In the first case, we assume that supercooled solution droplets (e.g., containing a small amount of sulfuric acid or other inorganic substances) freeze spontaneously (i.e., stochastically) to small ice crystals. The probability of a solution droplet of volume V freezing within a time interval Δt can be calculated as

$$P = 1 - \exp(-JV\Delta t), \tag{39}$$

with the nucleation rate J. For such solution droplets this rate can be formulated in terms of water activity,[21] which translates into the form

$$J(T, S_i) = J_0 \exp(A(T)(s - S_c(T))), \tag{40}$$

with a steepness $A(T)$ and a threshold $S_c(T)$. These two functions can be approximated by a recent formulation[22] to

$$A(T) \approx p_1(T) = a_{w0} + a_{w1} T, \tag{41}$$

$$S_c(T) \approx p_2(T) = a_{s0} + a_{s1} T + a_{s2} T^2, \tag{42}$$

using polynomials $p_n(x)$ of degree $n \in \mathbb{N}$.

There is still a debate about the relevance or dominance of these different nucleation pathways. However, for our purposes, we can restrict the formulation to homogeneous freezing of solution droplets since in the cold temperature regime of *in situ* formed ice clouds,[8] homogeneous nucleation produces most of the ice particles. Thus, we include a supersaturation limited pathway of ice nucleation.

For our model, we prescribe a size distribution of solution droplets. Instead of tracking aerosol properties with water uptake controlled by Köhler theory,[33] we use a lognormal distribution

with fixed modal radius and geometric standard deviation, normalized by the number concentration of aerosols. Details are given in Appendix A 2. This leads to a nucleation term Nuc_n for the ice crystal number concentration as given below. In addition, we assume a constant nucleation mass $m_{\mathrm{nuc}} = 10^{-16}$ kg (i.e., a radius of $\sim 0.3\,\mu$m) for each newly nucleated ice crystal, which gives the nucleation term Nuc_q for the mass concentration. In summary, we obtain

$$\mathrm{Nuc}_n = n_a V_{sol} J_0 \exp(p_{1e}(s - p_2)) = A_n \exp(p_{1e}(s - p_2)), \quad (43)$$

$$\mathrm{Nuc}_q = m_{\mathrm{nuc}} n_a V_{sol} J_0 \exp(p_{1e}(s - p_2)) = A_q \exp(p_{1e}(s - p_2)), \quad (44)$$

using two polynomials p_{1e}, p_2 depending on temperature solely (see Sec. III E and Appendix A 2), with a constant $A_n = n_a V_{sol} J_0$ for n_a, V_{sol}, J_0 as given in Appendix A 2 and $A_q = m_{\mathrm{nuc}} A_n$.

Since the mass of the newly nucleated ice particles is obtained from the surrounding water vapor (because the solution droplets deplete some water vapor), we introduce a sink term for the saturation ratio as

$$\mathrm{Nuc}_s = -A_s \exp(p_{1e}(s - p_2)) \quad \text{with } A_s = A_q \frac{p}{\varepsilon p_{\mathrm{si}}}, \quad (45)$$

where we use the approximation for saturation vapor pressure over hexagonal ice, p_{si}, as given in Appendix A 3; ε is again the ratio of molar masses of water and air $\varepsilon = \frac{M_{\mathrm{mol},v}}{M_{\mathrm{mol},d}} \approx 0.622$ as in Sec. III B.

3. Particle growth/evaporation by diffusion of water vapor

Small water particles (liquid or solid) grow by diffusion of surrounding water vapor through air. The boundary condition at the surface of the particle (i.e., saturation with respect to the phase of the particle) determines the direction of the water vapor flux, leading either to evaporation or growth of the particle. The mathematical details of the problem and a proof of uniqueness of the solution can be found in Baumgartner and Spichtinger.[34] The growth equation of a single water particle with mass m can be written as

$$\frac{\mathrm{d}m}{\mathrm{d}t} = 4\pi C D_v f_k G_v (s - 1) f_v. \quad (46)$$

The shape of the particle influences the diffusional growth; using the electrostatic analog,[31,34,35] a capacity coefficient C representing the shape of a single particle can be introduced to the growth equation. D_v denotes the diffusion coefficient of water vapor in air,

$$D_v = D_{v0} \left(\frac{T}{T_0}\right)^2 \left(\frac{p_0}{p}\right), \quad (47)$$

$$D_{v0} = 2.1422 \times 10^{-5}\ \mathrm{m}^2/\mathrm{s}, \quad (48)$$

$$T_0 = 273.15\ \mathrm{K}, \quad p_0 = 101\,325\ \mathrm{Pa}, \quad (49)$$

with a correction f_k of the flux in the kinetic regime; this correction would reduce the uptake of water vapor, since $f_k \leq 1$. The fit of D_v is based on the description by Hall and Pruppacher.[36] The effect of latent heat release is captured by the Howell factor

$$G_v = \left[\left(\frac{L}{R_v T} - 1 \right) \frac{L}{T} \frac{D_v}{K_T} + \frac{R_v T}{p_{si}} \right]^{-1}, \quad (50)$$

with the latent heat of sublimation L, the ideal gas constant of water vapor R_v, and the heat conduction of air K_T,[37] respectively. Note, that in this formulation we already omit possible corrections for small particles for D_v, K_T, respectively.[35] For large particles, a correction f_v for the ventilation effect (wakes behind falling particles enhance water vapor diffusion) is applied; this correction would enhance the uptake of water vapor, since $f_v \geq 1$.

Apart from the assumption of ice crystals of spherical shape, which leads to the radius as capacity factor $C = r$ [can be expressed as in Eq. (31) with the mean mass], we apply additional simplifications for the representation of the growth term:

- We neglect the ventilation correction for large particles, following the estimation by Ref. 35 that for spheres of radius smaller than $\sim 60\,\mu$m the correction is less than 20%, thus, we set $f_v = 1$. In Appendix A 6 some arguments for this approximation are presented.
- We neglect the kinetic correction, which would apply for very small ice particles, and especially affect nucleation events in clear air at very high velocities and/or low temperature regimes.[31] For our scenarios with pre-existing ice, the mean mass is usually large enough to omit this correction, i.e., we set $f_k = 1$. Details of the estimation are given in Appendix A 6.

Then, we can express the growth term for the mass concentration (see Appendix A 4 for the explicit calculation) as

$$\mathrm{Dep}_q = B_q n^{\frac{2}{3}} q^{\frac{1}{3}} (s - 1), \quad (51)$$

where

$$B_q = 4\pi G_v D_v c r_0^{-\frac{1}{9}} \quad (52)$$

with $c = \sqrt[3]{\frac{3}{4\pi\rho_b}}$ as in Eq. (31) and $r_0 = 3$ as set in Sec. III D.

The growth term models the transfer of water vapor to ice particles, thus we have to introduce a sink term for the saturation ratio, i.e.,

$$\mathrm{Dep}_s = -B_s n^{\frac{2}{3}} q^{\frac{1}{3}} (s - 1) \quad \text{with } B_s = B_q \frac{p}{\varepsilon p_{\mathrm{si}}}, \quad (53)$$

where again p_{si} is as given in Appendix A 3 and ε is the ratio of molar masses of water and air as in Sec. III B.

For the evaporation term of the number concentration, it is in fact quite tricky to introduce a meaningful ansatz for this term, since the type of the underlying distribution is changing by evaporation.[38] In this article, we concentrate on the supersaturated regime, thus we do not need to investigate the evaporation term in details for this study. For completeness however, we mention the following *ad hoc* ansatz:

$$\mathrm{Evap}_n = \frac{n}{q} \mathrm{Dep}_q H(1 - s) \quad (54)$$

with the assumption that the number concentration of ice crystals reduces proportionally to the loss of mass concentration. This only happens for subsaturation, thus a Heaviside function H is used for switching off the process at $s > 1$.

4. Sedimentation—A particle falls out due to gravity

Water particles in general, and also ice crystals are accelerated by gravity; since the friction of air leads to a drag and thus a balance of forces, ice crystals very quickly reach a so-called terminal velocity without any further acceleration. For low Reynolds numbers using the Stokes law[35] and assuming a spherical shape, the terminal velocity is proportional to the squared radius. For irregularly shaped particles as ice crystals, the terminal velocity can be approximated by power laws $v_t(m) = \alpha_k m^{\beta_k}$ with piecewise constant coefficients α_k, β_k.[31] We have to apply a correction factor,[31,39] taking into account the friction of the air at different densities, expressed as a function of temperature and pressure,

$$c(p,T) = \left(\frac{p}{p_c}\right)^{a_c}\left(\frac{T}{T_c}\right)^{b_c}, \tag{55}$$

$$p_c = 30\,000\ \text{Pa}, \quad T_c = 233\ \text{K}, \tag{56}$$

$$a_c = -0.178, \quad b_c = -0.394. \tag{57}$$

The terminal velocity of the ice particles as formulated in Spichtinger and Gierens[31] by piecewise power laws can be approximated by a simple approach

$$v_t(m) \approx v_{\text{final}} a_s m^{b_s} \frac{1}{v_{\text{final}} + a_s m^{b_s}}, \tag{58}$$

mimicking the major increase of the velocity. As discussed in Appendix A 6, the particles' radius is assumed to be smaller than $\sim 75\,\mu$m, thus we can make a further simplification

$$v_t(m) = a_s m^{\frac{2}{3}}, \quad a_s = 6 \times 10^5\ \text{m s}^{-1}\ \text{kg}^{-\frac{2}{3}}, \tag{59}$$

which is consistent with the expressions for falling spheres, i.e., the velocity is proportional to the squared radius.[35] The sedimentation is a vertical transport in a column. However, in our simple model, we concentrate on a single level and restrict ourselves to a box of a certain vertical extension Δz. Since we assume a homogeneous mixture of ice particles in the box, we can describe the change of the flux $j_\psi = \rho v_\psi \psi$ (for a quantity $\psi = n, q$) by the expression

$$\frac{\partial j_\psi}{\partial z} = \frac{j_\psi^{\text{top}} - j_\psi^{\text{bottom}}}{\Delta z}, \tag{60}$$

with the flux j_ψ^{top} through the top boundary into the box and the flux j_ψ^{bottom} through the bottom out of the box. Generally, we can only determine the outgoing flux, but we might add constraints for determining the incoming flux; otherwise, the incoming flux can be seen as a variable parameter. Thus, the sedimentation terms can be formulated as

$$\text{Sed}_n = F_n - \frac{1}{\Delta z} v_n n, \quad \text{Sed}_q = F_q - \frac{1}{\Delta z} v_q q, \tag{61}$$

with fluxes from above F_n, F_q. Using the approximation of the terminal velocity (59), and the formulation of general moments of the lognormal distribution (37), we can derive the averaged terminal velocities,

$$v_n = \frac{1}{n}\int_0^\infty f(m) v_t(m)\,\mathrm{d}m = \frac{1}{n}\left(a_s r_0^{-\frac{1}{9}} n^{\frac{1}{3}} q^{\frac{2}{3}}\right), \tag{62}$$

$$v_q = \frac{1}{q}\int_0^\infty f(m) m v_t(m)\,\mathrm{d}m = \frac{1}{q}\left(a_s r_0^{\frac{5}{9}} n^{-\frac{2}{3}} q^{\frac{5}{3}}\right), \tag{63}$$

and thus the sedimentation terms

$$\text{Sed}_n = F_n - \frac{1}{\Delta z} v_n n = F_n - C_n n^{\frac{1}{3}} q^{\frac{2}{3}}, \tag{64}$$

$$\text{Sed}_q = F_q - \frac{1}{\Delta z} v_q q = F_q - C_q n^{-\frac{2}{3}} q^{\frac{5}{3}}, \tag{65}$$

with the sedimentation constants

$$C_n = c(p,T)\frac{a_s r_0^{-\frac{1}{9}}}{\Delta z} \quad \text{and} \quad C_q = c(p,T)\frac{a_s r_0^{\frac{5}{9}}}{\Delta z}, \tag{66}$$

where $c(p,T)$ denotes the necessary correction factor for different pressures and temperatures as given in Eq. (55). The fluxes from above, F_n and F_q, appear as additional variables (or parameters). Since we would like to avoid too many parameters for our investigations, we adopt a strategy by Spichtinger and Czizco[40]: we assume that the sedimentation flux into the box/layer from above through the top boundary is a fixed fraction f_{sed} of the sedimentation flux through the bottom out of the box/layer, i.e., we set

$$j_\psi^{\text{top}} = f_{\text{sed}} \cdot j_\psi^{\text{bottom}}, \tag{67}$$

with a constant $0 \le f_{\text{sed}} \le 1$. The extreme values indicate either no flux into the box from above ($f_{\text{sed}} = 0$) or no net flux out of the box ($f_{\text{sed}} = 1$), i.e., the flux into the box from above and the flux out of the box are identical in magnitude. Thus, we find

$$F_n = f_{\text{sed}} C_n n^{\frac{1}{3}} q^{\frac{2}{3}}, \quad F_q = f_{\text{sed}} C_q n^{-\frac{2}{3}} q^{\frac{5}{3}}, \tag{68}$$

and set $F := 1 - f_{\text{sed}}$ for computational convenience later on with $0 < F \le 1$. We end with the final formulation of the sedimentation terms

$$\text{Sed}_n = -F C_n n^{\frac{1}{3}} q^{\frac{2}{3}}, \tag{69}$$

$$\text{Sed}_q = -F C_q n^{-\frac{2}{3}} q^{\frac{5}{3}}, \tag{70}$$

with F as explicit parameter in the terms. In our investigations, we set the vertical extension to $\Delta z = 100$ m, which is a typical extension of ice cloud layers[40,41] and is consistent with the assumption of a homogeneous cloud layer.

5. Collision of particles

Collision of particles is usually the major process for growing particles to large sizes. For liquid particles, collision is very efficient, but for pure ice particles in the cold temperature regime, aggregation is not a relevant process,[42,43] and we thus neglect it for our model.

6. Dependence of constants

The constants A_k, B_k, C_k $(k = n, q, s)$ in the model equations (4)–(6) depend all on p, T, whereas the constants D, p_{1e}, and p_2 just depend on T.

IV. QUALITATIVE PROPERTIES OF THE MODEL

In this section, we investigate the quality of the system in terms of theory of dynamical systems.

First, we show in IV A that there is always exactly one equilibrium point of the system and derive approximation formulas for this equilibrium point, and then study the quality of the equilibrium points in IV B. The results in those two subsections are derived by explicit calculations and mathematical arguments (under the additional assumption that the contribution to the change rates of q and s due to nucleation are neglectable as explained below).

Then, we use numerical methods to study limit cycles of the system in IV C and investigate scaling properties of the system in IV D.

A. Equilibrium states

We start with the determination of the equilibrium states of the system. Equilibrium points (stationary points/fixed points) of an ODE system are states for which the right-hand side of the ODE system vanishes, i.e., $\dot{n} = \dot{q} = \dot{s} = 0$, so we have to determine the roots of the 3D vector field $V(x)$.

First, note that we can omit the evaporation term

$$\mathrm{Evap}_n = B_q n^{\frac{5}{3}} q^{-\frac{2}{3}} (s-1) H(1-s) \tag{71}$$

from Eq. (4) since we are interested in the supersaturated regime (i.e., $s > 1$). Since we assume $w > 0$, this is not an approximation; the supersaturation source $A_s s$ always drives the system into states with $s > 1$, and thus $H(1-s) = 0$ and then also $\mathrm{Evap}_n = 0$.

Now, in order to (approximately) determine the equilibrium points, we make one more simplifying assumption. We estimate the contribution of the nucleation terms Nuc_q and Nuc_s to the changes rates of the mass concentration q and the saturation ratio s near an arbitrary equilibrium point and find that these terms are very small compared to the other terms as proven in Appendix B 1. Hence, we neglect the terms Nuc_q and Nuc_s in Eqs. (5) and (6) when determining equilibrium points of the system. Thus, we now have to find roots for the reduced system

$$\frac{\mathrm{d}n}{\mathrm{d}t} = A_n \exp(p_{1e}(s-p_2)) - FC_n n^{\frac{1}{3}} q^{\frac{2}{3}}, \tag{72}$$

$$\frac{\mathrm{d}q}{\mathrm{d}t} = B_q n^{\frac{2}{3}} q^{\frac{1}{3}} (s-1) - FC_q n^{-\frac{2}{3}} q^{\frac{5}{3}}, \tag{73}$$

$$\frac{\mathrm{d}s}{\mathrm{d}t} = Dw\, s - B_s n^{\frac{2}{3}} q^{\frac{1}{3}} (s-1). \tag{74}$$

This slight simplification has the convenient property that finding its roots can be reduced to finding the roots of a scalar function of the saturation ratio s. From this root s_0, the values of the equilibrium state (i.e., n_0, q_0) can be calculated recursively. The respective function for the saturation ratio is as follows (see Appendix B 2):

$$f(x) = ax - b(x-1)^{\frac{3}{4}} \exp\left(c(x-x_0)\right), \tag{75}$$

where

$$a = Dw, \quad b = \frac{B_s A_n}{C_n} \left(\frac{C_q}{B_q}\right)^{\frac{1}{4}} \left(\frac{1}{F}\right)^{\frac{3}{4}}, \quad c = p_{1e}, \quad x_0 = p_2. \tag{76}$$

For a given value of the saturation ratio s, we can calculate the respective values for n and q (see Appendix B 2) as

$$n = \frac{A_n}{FC_n} \exp(p_{1e}(s-p_2)) \left(\frac{B_q}{FC_q}(s-1)\right)^{-\frac{1}{2}} \tag{77}$$

and

$$q = \frac{A_n}{FC_n} \exp(p_{1e}(s-p_2)) \left(\frac{B_q}{FC_q}(s-1)\right)^{\frac{1}{4}}. \tag{78}$$

Next, we show that the 3D system has exactly one equilibrium point. For the existence of at least one root $s > 1$, we make the following argument: We investigate the function f from Eq. (75) on the interval $[1, \infty)$. For $s = 1$, we obtain $f(s) = a = Dw > 0$. Since the coefficients $a, b, c > 0$, the exponential term is the fastest growing one, such that $f(s) < 0$ for sufficiently large values of s. Then, the intermediate value theorem provides the existence of a root $s_0 > 1$. In order to see that f has exactly one root, we consider the function

$$g(x) = \frac{f(x)}{x} = a - bx^{-1}(x-1)^{\frac{3}{4}} \exp(c(x-x_0)) \tag{79}$$

and note that any $x = s > 1$ is a root of f if and only if x is a root of g. We calculate the derivative of g as

$$g'(x) = -bx^{-1}(x-1)^{\frac{3}{4}} \exp(c(x-x_0)) \cdot \left(c - \frac{1}{x}\right) - \frac{3}{4} bx^{-1}(x-1)^{-\frac{1}{4}} \exp(c(x-x_0)). \tag{80}$$

Since $c = p_{1e}(T) > 1$ in the considered temperature range, we can conclude that $g'(x) < 0$ for all $x > 1$, i.e., g is strictly decreasing for $x > 1$ and thus there is at most one root. Altogether, we conclude that there is exactly one root s_0 of f and thus exactly one equilibrium point of system (72)–(74).

We now want to derive a meaningful approximation of the equilibrium states. Let s_0 denote the saturation ratio at the equilibrium point for a given vertical velocity w (and fixed temperature, pressure, and sedimentation parameter). Then, we have

$$as_0 = b(s_0-1)^{\frac{3}{4}} \exp(c(s_0-x_0)) \tag{81}$$

and hence, using $c = p_{1e}$, $x_0 = p_2$, we get

$$s_0 = p_2 + \frac{1}{p_{1e}} \log\left(a \cdot b^{-1} \cdot s_0 (s_0-1)^{-\frac{3}{4}}\right). \tag{82}$$

Plugging in the definitions for a and b, we get for s_0 at the equilibrium point

$$s_0 = p_2 + \frac{1}{p_{1e}} \log\left(D \frac{C_n}{B_s A_n} \left(\frac{B_q}{C_q}\right)^{\frac{1}{4}}\right) + \frac{1}{p_{1e}} \log\left(w \cdot F^{\frac{3}{4}} \cdot s_0 (s_0-1)^{\frac{3}{4}}\right). \tag{83}$$

Motivated by this calculation, we define the functions

$$\sigma(T,p) := p_2 + \frac{1}{p_{1e}} \log\left(D \frac{C_n}{B_s A_n} \left(\frac{B_q}{C_q}\right)^{\frac{1}{4}}\right) \tag{84}$$

and

$$h(x) := h(x, F, w, T, p)$$
$$= \sigma + \frac{1}{p_{1e}} \left(\log(w) + \frac{3}{4} \log(F) + \log \left(\frac{x}{(x-1)^{\frac{3}{4}}} \right) \right) \quad (85)$$

such that the above s_0 satisfies $s_0 = h(s_0, F, w, T, p)$. More generally, a direct calculation shows that x^* is a fixed point of h (i.e., $x^* = h(x^*)$) if and only if x^* is a root of f (i.e., $f(x^*) = 0$). Therefore, fixed points x^* of h correspond to the values of the saturation ratio at equilibrium points of the ice cloud model.

We now show that the function h is furthermore a contraction on a suitable compact interval (which in turn narrows the range for the equilibrium value s_0) and use this property for a suitable approximation. Estimating the ranges of the functions σ and p_{1e} (see Appendix C), we find

$$h(x) = \kappa_0 + \frac{1}{p_{1e}} \log \left(\frac{x}{(x-1)^{\frac{3}{4}}} \right) \quad (86)$$

for some (variable) $\kappa_0 \in [1.375\,170, 1.585\,966]$. Let us now specify the following interval:

$$[s_{\min}, s_{\max}] \quad \text{with } s_{\min} = 1.37, \quad s_{\max} = 1.59. \quad (87)$$

We can show (see Appendix C) that

$$h([s_{\min}, s_{\max}]) \subset [s_{\min}, s_{\max}]. \quad (88)$$

In addition, we calculate the derivative of h as

$$h'(x) = \frac{1}{4p_{1e}} \frac{x-4}{x(x-1)} \quad (89)$$

and thus,

$$|h'(x)| \leq \frac{\pi_2}{4} \frac{4 - s_{\min}}{s_{\min}(s_{\min} - 1)} \approx 0.004\,415 \ll 1, \quad (90)$$

with $\frac{1}{p_{1e}} \leq \pi_2 = 0.003\,404$ as in Appendix C. Therefore, h is a contraction on the compact interval $[s_{\min}, s_{\max}] \subset \mathbb{R}$. Consequently, the Banach fixed point theorem yields the existence of a unique fixed point, and the sequence x_n defined by

$$x_n = h(x_{n-1}) = \sigma + \frac{1}{p_{1e}} \log(w) + \frac{3}{4p_{1e}} \log(F) + \frac{1}{p_{1e}} \log \left(\frac{x_{n-1}}{(x_{n-1} - 1)^{\frac{3}{4}}} \right) \quad (91)$$

converges to this fixed point s_0. This implies in particular that the saturation ratio s_0 at an equilibrium point [which has the value of the unique fixed point of $h(x)$] is always contained in the interval $[s_{\min}, s_{\max}]$ for any given environmental conditions in the relevant ranges as previously specified and summarized in Table I.

In practice, we can determine an approximation for the value of s_0 while approximating the function $l(x) = \log \left(\frac{x}{(x-1)^{\frac{3}{4}}} \right)$ on the interval $[s_{\min}, s_{\max}]$ by the midpoint of possible values $\ell_m = \frac{1}{2}(l(s_{\min}) + l(s_{\max})) \approx 0.959\,979$, such that

$$s_0 \approx \sigma(T, p) + \frac{1}{p_{1e}(T)} \left(\ell_m + \log(w) + \frac{3}{4} \log(F) \right), \quad (92)$$

with an absolute error of approximation smaller than 4×10^{-4}. Hence, the proof of uniqueness using the fixed point theorem also leads to an approximate description of the equilibrium states as a by-product in our setting here. Note here, that the contraction property assures that the approximation converges toward the equilibrium point, i.e., iteration of the function leads to an improved approximation.

Using Eqs. (77) and (78) for the calculation of the other values of the equilibrium state n_0, q_0 from the value s_0, we finally get the equations

$$n_0 = \frac{D}{B_s} \left(\frac{C_q}{B_q} \right)^{\frac{1}{4}} \cdot w \cdot F^{\frac{1}{4}} \cdot s_0 (s_0 - 1)^{-\frac{5}{4}}, \quad (93)$$

$$q_0 = \frac{D}{B_s} \left(\frac{B_q}{C_q} \right)^{\frac{1}{2}} \cdot w \cdot F^{-\frac{1}{2}} \cdot s_0 (s_0 - 1)^{-\frac{1}{2}}. \quad (94)$$

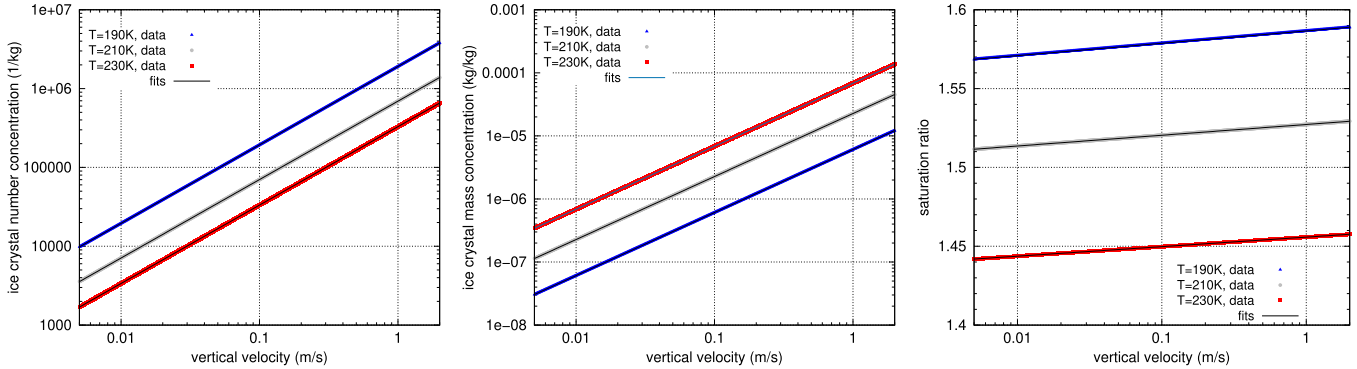

FIG. 1. Equilibrium states for the ice cloud model at $p = 300$ hPa. Colors indicate different temperatures, i.e., red: 230 K, gray: 210 K, blue: 190 K. Black lines indicate approximations as given in Eqs. (92)–(94). Left: Number concentration (in 1/kg), middle: mass concentration (in kg/kg), right: saturation ratio.

Since the changes in the saturation ratio s_0 at the equilibrium point for varying w and F within the specified ranges are only very minor compared to the changes in w and $F^{\frac{1}{4}}$ or $F^{-\frac{1}{2}}$ in Eqs. (93) and (94) [due to the low values of $\frac{1}{p_{1e}(T)}$ as specified in Eqs. (C2) and (C4)], good approximations for the ice crystal number and mass concentrations n_0 and q_0 at the equilibrium point for varying w and F are given by calculating s_0 for one choice of vertical velocity w and sedimentation parameter F (e.g., for $w = 0.1\,\mathrm{m\,s^{-1}}$ and $F = 1.0$) and then approximating n_0 and q_0 by Eqs. (93) and (94) using the fixed s_0. In Fig. 1, the equilibrium states for different temperatures are represented. The dependency of all quantities n, q, s on $\log(w)$ is clearly visible, since we use a logarithmic axis for the vertical updrafts. The quasi-linear fits are almost perfect.

B. Quality of equilibrium states

The quality of the equilibrium point of the model depends on the choice of the parameters and can be deduced from the eigenvalues of the Jacobi matrix of the system at the equilibrium point; this is true at least in case of non-zero eigenvalues, which is the case here, as we show later. The Jacobi matrix of the reduced system (72)–(74) at an arbitrary point (n, q, s) is given by

$$J = \begin{pmatrix} -\frac{1}{3}FC_n\bar{m}^{\frac{2}{3}} & -\frac{2}{3}FC_n\bar{m}^{-\frac{1}{3}} & p_{1e}A_n\exp(p_{1e}(s-p_2)) \\ \frac{2}{3}\left(B_q\bar{m}^{\frac{1}{3}}(s-1)+FC_q\bar{m}^{\frac{5}{3}}\right) & \frac{1}{3}B_q\bar{m}^{-\frac{2}{3}}(s-1)-\frac{5}{3}FC_q\bar{m}^{\frac{2}{3}} & B_q n^{\frac{2}{3}}q^{\frac{1}{3}} \\ -\frac{2}{3}B_s\bar{m}^{\frac{1}{3}}(s-1) & -\frac{1}{3}B_s\bar{m}^{-\frac{2}{3}}(s-1) & Dw - B_s n^{\frac{2}{3}}q^{\frac{1}{3}} \end{pmatrix}. \tag{95}$$

Here, $\bar{m} = \frac{q}{n}$ denotes the mean mass of ice crystals. Since the expressions become too complicated there is no chance to calculate the eigenvalues analytically at the equilibrium points. However, we can partly determine the general quality of the solution, e.g., properties such as the sign of the eigenvalues. For this purpose, we reformulate the Jacobi matrix.

Using the conditions for an equilibrium point, i.e., $(\dot{n}, \dot{q}, \dot{s}) = (0, 0, 0)$, we obtain the following equations (see Appendix B 2):

$$A_n\exp(p_{1e}(s-p_2)) = FC_n n^{\frac{1}{3}}q^{\frac{2}{3}}, \tag{96}$$

$$\bar{m} = \left(\frac{B_q}{FC_q}(s-1)\right)^{\frac{3}{4}}, \tag{97}$$

$$B_s(s-1) = Dw\,s\bar{m}^{-\frac{1}{3}}n^{-1}. \tag{98}$$

These identities can be used for rewriting the Jacobi matrix as

$$J = \begin{pmatrix} -\frac{1}{3}FC_n\bar{m}^{\frac{2}{3}} & -\frac{2}{3}FC_n\bar{m}^{-\frac{1}{3}} & p_{1e}FC_n\bar{m}^{\frac{2}{3}}n \\ \frac{4}{3}FC_q\bar{m}^{\frac{5}{3}} & -\frac{4}{3}FC_q\bar{m}^{\frac{2}{3}} & \frac{1}{(s-1)}FC_q\bar{m}^{\frac{5}{3}}n \\ -\frac{2}{3}Dwsn^{-1} & -\frac{1}{3}Dwsq^{-1} & -Dw\frac{1}{(s-1)} \end{pmatrix}. \tag{99}$$

It turns out that this matrix J is similar to a slightly simpler matrix J_1, which has the same eigenvalues, i.e., $J = D_m^{-1}J_1D_m$, and finally, $J = a\cdot D_m^{-1}J_2D_m$, with

$$a = \frac{1}{3}FC_n\bar{m}^{\frac{2}{3}}, \quad D_m = \begin{pmatrix} 1 & 0 & 0 \\ 0 & \bar{m}^{-1} & 0 \\ 0 & 0 & n \end{pmatrix}, \tag{100}$$

$$J_2 = \begin{pmatrix} -1 & -2 & 3p_{1e} \\ 4r_0^{\frac{2}{3}} & -4r_0^{\frac{2}{3}} & 3r_0^{\frac{2}{3}}\frac{1}{(s-1)} \\ -2\gamma\frac{s}{\sqrt{s-1}} & -\gamma\frac{s}{\sqrt{s-1}} & -3\gamma\frac{1}{(s-1)^{\frac{3}{2}}} \end{pmatrix}, \tag{101}$$

using the relations

$$C_q = r_0^{\frac{2}{3}}C_n, \quad \gamma = DwF^{-\frac{1}{2}}B_q^{-\frac{1}{2}}r_0^{\frac{1}{3}}C_n^{-\frac{1}{2}}. \tag{102}$$

For the calculation of the determinant we use the formulation $J = a\cdot D_m^{-1}J_2D_m$, thus we find

$$\det J = \frac{1}{3}F^2C_n^2Dw\bar{m}^{\frac{4}{3}}r_0^{\frac{2}{3}}\frac{1}{s-1}\cdot(-4+s-4s(s-1)p_{1e}). \tag{103}$$

Since $F, C_n, D, w, \bar{m}$ are all positive and $s > 1$ and $p_{1e} > 1$ in the considered range, we find

$$-4+s-4s(s-1)p_{1e} = -3+(s-1)(-4sp_{1e}+1) < 0$$
$$\Rightarrow \det J < 0.$$

Let $\lambda_1, \lambda_2, \lambda_3$ denote the eigenvalues of J for a given equilibrium state. After rearranging/renumbering, we can assume that either all eigenvalues are real or one (λ_3) is real and two are complex conjugates ($\lambda_1 = \lambda_2^*$). Since $\det J = \lambda_1\lambda_2\lambda_3 < 0$, we conclude that there has to be at least one negative real eigenvalue $\lambda_i < 0$. In addition, all eigenvalues are non-zero ($\lambda_i \neq 0$ for all $i = 1, 2, 3$).

The eigenvalues are then calculated numerically using routines of the package "linalg" in "numpy."[44] The real negative eigenvalue is denoted by λ_3. For most parameters, we find two complex-conjugate eigenvalues λ_1, λ_2; in a small regime (higher temperature and very low vertical velocities), we obtain two real negative eigenvalues $\lambda_1, \lambda_2 < 0$. We find two supercritical Hopf bifurcations of the system, i.e., the real part of the complex-conjugate eigenvalues changes its sign, such that there is a transition from a stable

equilibrium point to the case of an unstable equilibrium point and an attracting limit cycle.[45] For the local existence of the periodic solutions (i.e., limit cycles), we can apply a theorem based on Lyapunov–Schmidt reduction,[46] since at the bifurcation point we have exactly two conjugate imaginary eigenvalues and no other eigenvalues on the imaginary axis. However, we will investigate the limit cycles later in Sec. IV C, using numerical investigations.

Using the description of the trace of the Jacobi matrix, we can derive additional properties of the eigenvalues of the linearized system. The trace can be calculated as

$$\begin{aligned}\mathrm{tr}(J) &= \mathrm{tr}\left(aD_m^{-1}J_2D_m\right) = a\mathrm{tr}(J_2)\\ &= -a\left(1+4r_0^{\frac{2}{3}}+3\gamma\frac{1}{(s-1)^{\frac{3}{2}}}\right),\end{aligned} \tag{104}$$

using the description of the matrix J_2 in Eq. (101). Since the constants a, r_0, γ are all positive and in the considered range we have $s > 1$, we find a negative trace of the Jacobi matrix

$$\mathrm{tr}(J) = a\mathrm{tr}(J_2) = \lambda_1+\lambda_2+\lambda_3 < 0. \tag{105}$$

This condition can be reformulated as $\lambda_1+\lambda_2 < -\lambda_3$ with the distinct real and negative eigenvalue $\lambda_3 \in \mathbb{R}_{<0}$. We can distinguish different cases

1. For a pair of complex-conjugate eigenvalues $\lambda_1 = \lambda_2^* = \alpha + i\beta \in \mathbb{C}$ $(\alpha, \beta \in \mathbb{R})$, we find

$$\lambda_1+\lambda_2 = 2\alpha < -\lambda_3 \tag{106}$$

$$\Leftrightarrow \alpha = \mathrm{Re}(\lambda_{1,2}) < -\frac{\lambda_3}{2} \in \mathbb{R}_{>0}. \tag{107}$$

   For negative real parts α this is not a restriction, since then we find $\alpha < 0 < -\frac{\lambda_3}{2}$. However, for positive real parts (i.e., in case of an unstable fixed point), we determine the condition $0 < \alpha < -\frac{\lambda_3}{2}$. Thus, the absolute value of the growth rate $\mathrm{Re}(\lambda_{1,2}) = \alpha$ of the instability close to the equilibrium point is always smaller than the value of the contraction rate λ_3, i.e., close to the equilibrium state the flow contraction in λ_3-direction is always faster than the blowup in $\lambda_{1,2}$-directions. This points to a quasi 2D system for longer time scales.
2. For real eigenvalues $\lambda_1, \lambda_2 \in \mathbb{R}$, we still have the property $\lambda_1+\lambda_2 < -\lambda_3$. In the numerical determination we only find the case of two negative real eigenvalues $\lambda_1, \lambda_2 < 0$; thus, there is again no restriction for the eigenvalues, since the eigenvalues always fulfill $\lambda_1+\lambda_2 < 0 < -\lambda_3$.

In Fig. 2, we show an example of real and imaginary parts of the numerically determined eigenvalues for a fixed parameter set of $p = 300$ hPa, $T = 230$ K, $F = 1$ and values of vertical updrafts in the interval $0.0005 \le w \le 2\,\mathrm{m\,s^{-1}}$. Note, that we show a regime with all possible occurring variants of eigenvalues, i.e., conjugate-complex pair and three real eigenvalues. For the unstable regime (for positive real part, i.e., in the range between $w \sim 0.048$ and $w \sim 0.77\,\mathrm{m\,s^{-1}}$) we clearly see, that the relation (107) is fulfilled, i.e., the positive real part of $\lambda_{1,2}$ is much smaller than the absolute value of λ_3.

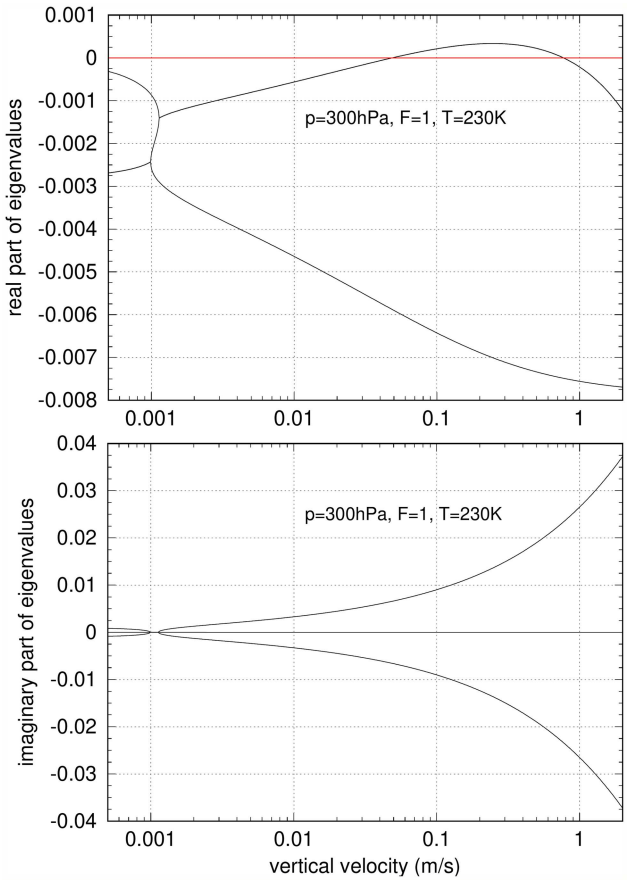

FIG. 2. Example of real (top) and imaginary (bottom) parts of determined eigenvalues at the equilibrium state of the system for a fixed set of parameters $p = 300$ hPa, $T = 230$ K, $F = 1$.

Remark: If we could assure that the real part of the complex-conjugate eigenvalues changes with non-zero speed at the bifurcation points, a theorem by Hopf[47] would guarantee the existence of a two dimensional center manifold, on which the limit cycle lies.

We calculate the bifurcation points numerically. For a fixed temperature T, we scan through the w-interval, calculate the eigenvalues of the respective Jacobi matrix J, and determine the position where the sign of the real part of $\lambda_{1,2}$ changes. The bifurcation diagram for values $p = 300$ hPa and $F = 1$ is represented in Fig. 3. Blue and red dots mark the numerically determined Hopf bifurcations, gray dots mark the region of three real and negative eigenvalues.

We find that the two bifurcations for $F = 1$ can be fitted using exponential functions with quadratic polynomials in the argument, i.e., functions of the form

$$w_a(T) = \bar{w}\exp\left(a_2T^2+a_1T+a_0\right), \tag{108}$$

$$w_b(T) = \bar{w}\exp\left(b_2T^2+b_1T+b_0\right), \tag{109}$$

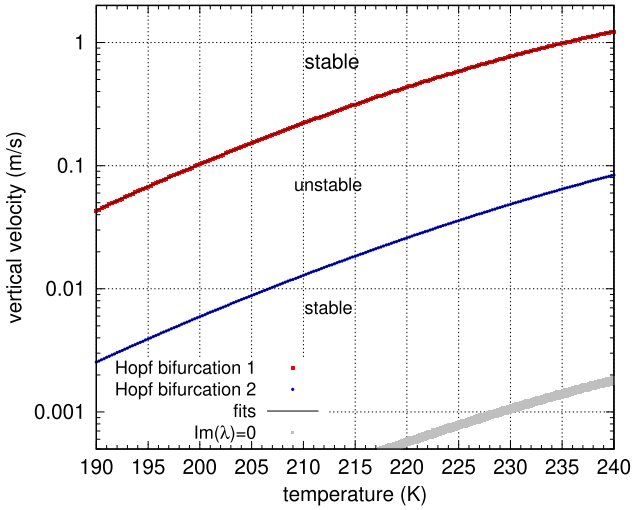

FIG. 3. Bifurcation diagram in the parameter space $T - w$ for $p = 300$ hPa and $F = 1$. The red and blue dots indicate the numerically calculated transition in the real parts of the complex-conjugate eigenvalues $\lambda_{1,2}$, i.e., the two Hopf bifurcations. The black lines indicate fits to the bifurcations using a quadratic polynomial in T. Above the red points and below the blue points, the unique equilibrium state is stable. Between the two lines, the equilibrium state is unstable and a limit cycle occurs. Gray dots indicate the region with purely real eigenvalues (i.e., three negative real eigenvalues).

with coefficients a_i, b_i as represented in Table II, and the "constant" $\bar{w} = 1\,\mathrm{ms}^{-1}$ determining the correct unit of the functions. The fits are shown in Fig. 3 as black lines; however, blue dots "belong" to fit $w_a(T)$, whereas red dots "belong" to fit $w_b(T)$. The bifurcation diagram for other values of F will be discussed later in the Sec. IV D, where we investigate the scaling properties of the system. For different values of pressure (i.e., $p = 200$ hPa) we find qualitatively similar bifurcation diagrams, i.e., the supercritical Hopf bifurcations are still there, however, slightly shifted in their position. In fact, the quality of the system stays the same.

Remark: For the Jacobi matrix at the equilibrium state at the bifurcation, we can use basic relations from linear algebra

$$\lambda_{1,2} = \pm i\beta \;\Rightarrow\; \mathrm{tr}(J) = \lambda_3 \;\Rightarrow\; \det(J - \lambda_3 I) = 0 \tag{110}$$

TABLE II. Coefficients for the quadratic fit functions $w_a(T)$, $w_b(T)$ of the two Hopf bifurcations.

	$k=0$	$k=1$	$k=2$
a_k	−38.309 47	0.278 555 K^{-1}	−0.000 491 91 K^{-2}
b_k	−36.150 46	0.229 111 K^{-1}	−0.000 369 97 K^{-2}

to derive a quasi-quadratic equation from the determinant for the bifurcation value w, i.e.,

$$\alpha_2 w^2 + \alpha_1 w + \alpha_0 = 0 \tag{111}$$

with coefficients $\alpha_2, \alpha_1, \alpha_0$ only slightly depending on w. This gives also an analytical hint, that we should find two bifurcations for the system. When calculating the values of w from Eq. (111), we find values very close to the bifurcation points as numerically calculated from the complete system.

In Fig. 4, some examples for the three different regimes are represented, i.e., the time evolution of the saturation ratio s is shown for values $w = 0.01\,\mathrm{m\,s}^{-1}$ (stable equilibrium, lower regime), $w = 0.1\,\mathrm{m\,s}^{-1}$ (unstable equilibrium, limit cycle), and $w = 1\,\mathrm{m\,s}^{-1}$ (stable equilibrium, higher regime). In all simulations, we see the same general evolution of a first and undisturbed nucleation event followed by a (more or less) strong reduction of the supersaturation, and afterward subsequent nucleation events, which are less vigorous since pre-existing ice slows down the explosion term. This behavior was observed in former studies.[40] All variables of the simulations are shown in Appendix D, i.e., Figs. 11, 12, and 13.

Qualitatively, we can describe the behavior with the three different processes. Nucleation, as driven by the cooling/forcing term of s, acts as a source for ice crystals, whereas sedimentation is the sink for ice crystals. The growth process acts as a mediator in between, shifting mass from the saturation ratio to the mass concentration, which (1) shuts down the nucleation event because of less supersaturation as discussed in Spichtinger and Krämer[48] and (2) enhances the sedimentation sink. This feedback can also be seen calculating the divergence of the vector field, i.e., the trace of the general Jacobi matrix,

$$\nabla \cdot V = \mathrm{tr}(J) = Dw + \frac{1}{3} B_q \bar{m}^{-\frac{2}{3}} (s-1) - B_s n \bar{m}^{\frac{1}{3}} - \frac{1}{3} F C_n \left(1 + 5 r_0^{\frac{2}{3}}\right) \bar{m}^{\frac{2}{3}}. \tag{112}$$

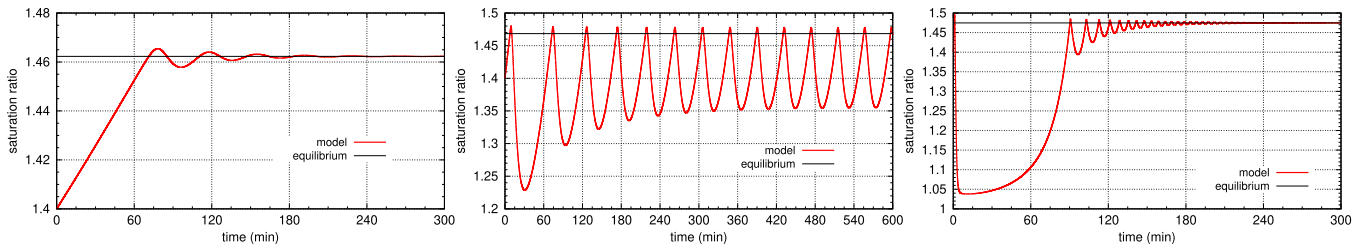

FIG. 4. Examples of solutions for different regimes at $T = 225$ K, $p = 300$ hPa, and $F = 1$; the saturation ratio s is displayed. Left: damped oscillator ($w = 0.01\,\mathrm{m\,s}^{-1}$), middle: undamped oscillator ($w = 0.1\,\mathrm{m\,s}^{-1}$), right: damped oscillator ($w = 1\,\mathrm{m\,s}^{-1}$).

The first term, i.e., the cooling/forcing of the system is clearly positive, the last term, i.e., sedimentation, is negative, and the growth terms in the middle could change signs. For small particles, the first term of growth dominates (positive), whereas for large (or many) particles, the second term of growth dominates (negative). However, the divergence can change sign, thus a clear asymptotic behavior cannot be seen from this analysis.

As described in Sec. IV C, in the unstable case, we observe an undamped oscillation, which indicates an attracting limit cycle.

C. Limit cycles

There is no method available for calculating the limit cycles, or even their periods analytically for this 3D nonlinear system, at least to our best knowledge. Therefore, we use a numerical method to determine the period of the limit cycles. For this purpose, we integrate the system again for quite a long time but with initial conditions close to the unstable equilibrium state. To be precise, for a (numerically determined) equilibrium point $x_0 = (n_0, q_0, s_0)^T$, we determine the initial condition as $x_{\text{init}} = x_0 \cdot (1 - \varepsilon)$ with a small deviation $\varepsilon = 0.01$. We then run the simulation for a time T_{final}, which is approximately determined as $T_{\text{final}} = 300 \cdot \tau_\lambda$ with the period at the equilibrium point $\tau_\lambda = \frac{2\pi}{\text{Im}(\lambda_1)}$, using the imaginary part of the two complex-conjugate eigenvalues. The simulations are carried out using a Gaussian grid with a timestep, adaptively but constant determined by the empirical relation[31] $\Delta t = \frac{0.01\,\text{m}}{w}$, using the prescribed vertical velocity w.

Since the variable s is the most "linear" one, we then determine minima and maxima of this variable over time. From the difference between consecutive minima or maxima, respectively, at the end of the simulation, we determine two periods $\tau_{\text{min}}, \tau_{\text{max}}$. The mean value $\tau = \frac{1}{2}(\tau_{\text{min}} + \tau_{\text{max}})$ is then used as the numerically determined period of the limit cycle, for a given set of parameters (p, T, w, F), respectively. In Fig. 5 (top panel), the periods of the limit cycles are represented. For the domain between the two Hopf bifurcations, the color code indicates the periods of the limit cycles. Note that there is a huge range of periods, ranging from very short periods at high temperatures and high vertical velocities (in the order of few hundreds of seconds) up to large periods at low temperatures and low vertical updrafts (in the order of 10^4 to 10^5 s). The periods depending on w show a similar shape for a distinct temperature, as will be investigated later in terms of scaling properties in Sec. IV D. In the bottom panel of Fig. 5, an example for periods at a fixed temperature of $T = 210$ K, but varying vertical updraft, is displayed. The red curve shows the "oscillation period" as derived from the imaginary part of the respective complex-conjugate eigenvalues $\left(\tau = \frac{2\pi}{\text{Im}(\lambda_k)}\right)$ at the equilibrium point, whereas the black curve shows the period of the limit cycle in the region of the unstable equilibrium point. Both curves touch each other at the bifurcation, as expected. The periods of the limit cycle always have a distinct maximum in the interval between the two bifurcation lines. Note that for the small regime of three real eigenvalues, as indicated in Fig. 3 by the gray shading, τ shows a singularity when approaching an imaginary part $\text{Im}(\lambda_k) = 0$.

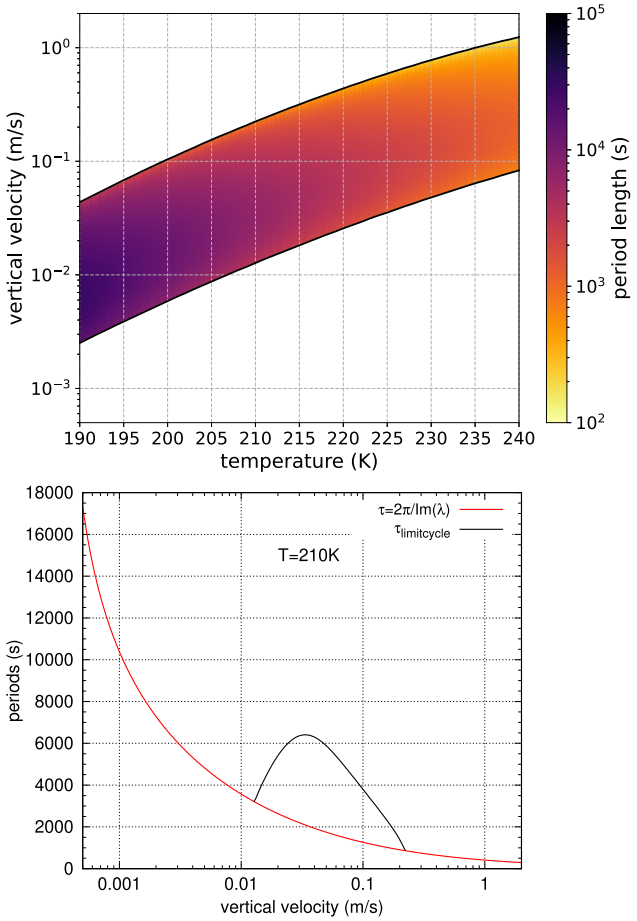

FIG. 5. Top: Periods of limit cycles in the bifurcation diagram. Bottom: Example of section through the parameter space at fixed temperature $T = 210$ K, representing the oscillation period as calculated from the imaginary part of the complex eigenvalues (red line), and the period of the respective limit cycle in the unstable regime (black line).

D. Scaling properties

Now, we investigate some scaling properties of the system using numerical methods.

1. Scaling property of bifurcations

Until now, we investigated the bifurcations for variations in p, T, w, but left the sedimentation parameter unchanged, i.e., $F = 1$ (no flux from above). Now, we investigate possible changes in the bifurcations due to variation of F in the interval $0.01 < F < 1$. This is a realistic range; smaller values do not make sense because then we would effectively shut down the sedimentation sink, which is the crucial process for producing an oscillating behavior. In addition to the numerical calculations of the equilibrium states, the linearization and eigenvalues leading to the bifurcations as determined by the numerical procedure, we evaluate the variation in a semi-analytical approximate way.

We investigate pairs of bifurcation coordinates (w, F) for fixed values of the environment p, T. First, suppose that we have already determined a bifurcation point (w_0, F_0), i.e., for the Jacobi matrix at the equilibrium state we find eigenvalues $\lambda_1 = \lambda_2^* = i\beta$, and for small perturbations their real parts change the sign. Let us now show that we can approximately determine another bifurcation point (w_1, F_1) just from the original pair (w_0, F_0) via the Jacobi matrix. Here, we observe that beside the actual values of the equilibrium state and the sedimentation parameter F only the constants D, B_q, C_n, p_{1e} impact the value of the Jacobi matrix, which are all independent of w and F.

We try to find another pair (w_1, F_1) close to the original one, i.e., we apply a small perturbation to w and F. From the approximation in Eq. (92), we see that the value of s does not change substantially for moderate/small variations in w and/or F. Thus, from the special form of the Jacobi matrix J_2, we might assume that in a first approximation, J_2 changes only in γ via changes in $DwF^{-\frac{1}{2}}$ [see Eq. (102)], when varying updraft and sedimentation parameter. Hence, passing to a different sedimentation parameter F_1 and a vertical velocity w_1, we observe that γ and consequently J_2 are approximately equal for (w_0, F_0) and (w_1, F_1) if and only if

$$Dw_0F_0^{-\frac{1}{2}} = Dw_1F_1^{-\frac{1}{2}} \Leftrightarrow \frac{w_0}{w_1} = \left(\frac{F_0}{F_1}\right)^{\frac{1}{2}}. \tag{113}$$

Now, we consider the "special case" of setting $F_0 = 1$. Thus, we obtain

$$\frac{w_0}{w_1} = \left(\frac{1}{F_1}\right)^{\frac{1}{2}} \Leftrightarrow w_1 = F_1^{\frac{1}{2}} w_0 = \sqrt{F_1} w_0 \tag{114}$$

and for a bifurcation point $(w_0, 1)$ also the pair $(\sqrt{F_1}w_0, F_1)$ is (approximately) a bifurcation point, so we get a scaling of the updrafts by the square root of the sedimentation parameter. However, this relation relies on small perturbations and approximations, so one would like to evaluate the "real" values of bifurcations as determined numerically with the procedure explained above. These bifurcation values are displayed as black dots in Fig. 6. In Sec. IV B, we found fits for the bifurcation points ($F = 1$) of the form

$$w(T) = \bar{w} \exp\left(c_0 + c_1 T + c_2 T^2\right). \tag{115}$$

On the other hand, from the (semi-)analytical description above, we know that approximately $w_1 = \sqrt{F} w_0$. For evaluating this approximation, we make the general ansatz of a power law for the scaling, i.e., $w_1 = F^\alpha w_0$ with a positive real number $\alpha \in \mathbb{R}_{>0}$. Then, we can derive

$$\begin{aligned} w_1(T) = F^\alpha w_0(T) &= F^\alpha \bar{w} \exp\left(c_0 + c_1 T + c_2 T^2\right) \\ &= \bar{w} \exp\left(\bar{c}_0 + c_1 T + c_2 T^2\right), \end{aligned} \tag{116}$$

with $\bar{c}_0 = \alpha \log(F) + c_0$.

We determine fits for sedimentation factors $F \in \{0.01, 0.02, 0.05, 0.1, 0.2, 0.3, 0.4, 0.5, 0.6\}$ for both bifurcations and determine the exponent α (also in terms of a mean value). We find for the upper bifurcation $\alpha \approx \frac{1}{2}$ as from theory, whereas for the lower bifurcation, the values changes slightly to $\alpha \approx 0.512 \approx \frac{1}{2}$. Thus, the scaling property of the bifurcation due to F^α is a robust feature. In Fig. 6, the scaled fits using the respective ansatz $w(T) = F^\alpha w_*(T)$ are shown for

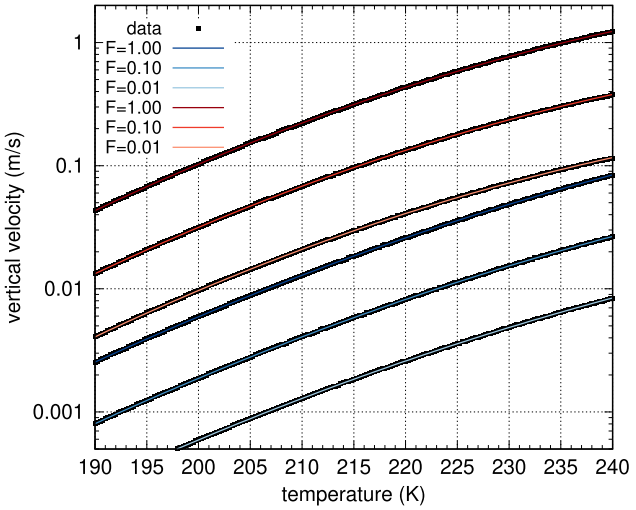

FIG. 6. Scaling of bifurcations for different values of the sedimentation parameter F. Black dots show the numerically derived values, whereas colored lines represent the scaling of the fit curves as derived for the parameter $F = 1$. Reddish colors show the change in the upper bifurcation, whereas bluish colors show the change in the lower bifurcations; in both cases, sedimentation parameters of $F = 1, 0.1, 0.01$ are shown.

$F = 1, 0.1, 0.01$; reddish colors show the upper bifurcations, whereas bluish colors display the lower bifurcation. The fits match the data points quite well, corroborating this type of scaling. Finally, we can state that the change of the sedimentation parameter F does not change the quality of the bifurcation diagram. Actually, the quality of the phase diagram and thus the bifurcations remain the same, only the transition lines/bifurcation curves change their position, but even not their shape.

2. Scaling property of limit cycle periods

In Sec. IV C, we determined the periods of the limit cycles for the regime of unstable equilibrium states. We already noted that the shape of the curves at fixed but different temperatures T is very similar. In the left panel of Fig. 7, the curves for the periods of the limit cycles at different temperatures are displayed. In the double-logarithmic representation the similarity of the curves is very evident. Thus, we make an empirical scaling ansatz, using the temperature value $T_{\text{ref}} = 210\,\text{K}$ as reference temperature. We hypothesize that the curves scale with a non-dimensional temperature. Using the reduced temperature $x := \frac{T}{T_{\text{ref}}}$, we might find scaling functions $f(x), g(x)$ such that the periods $\tau(w, T)$ can be expressed as

$$\tau\,(w, T) = f(x)\tau\left(g(x)w, T_{\text{ref}}\right). \tag{117}$$

The scaling function $g(x)$ shifts the w-position of the periods, whereas the function $f(x)$ changes the amplitude of the periods, respectively. This kind of scalings are often found in phase transitions and self-organized criticality,[49] and thus, we would expect a function of the form $f(x) \sim x^a$ with a so-called critical exponent $a \in \mathbb{R}$. A similar form is expected for the function $g(x)$. Comparing

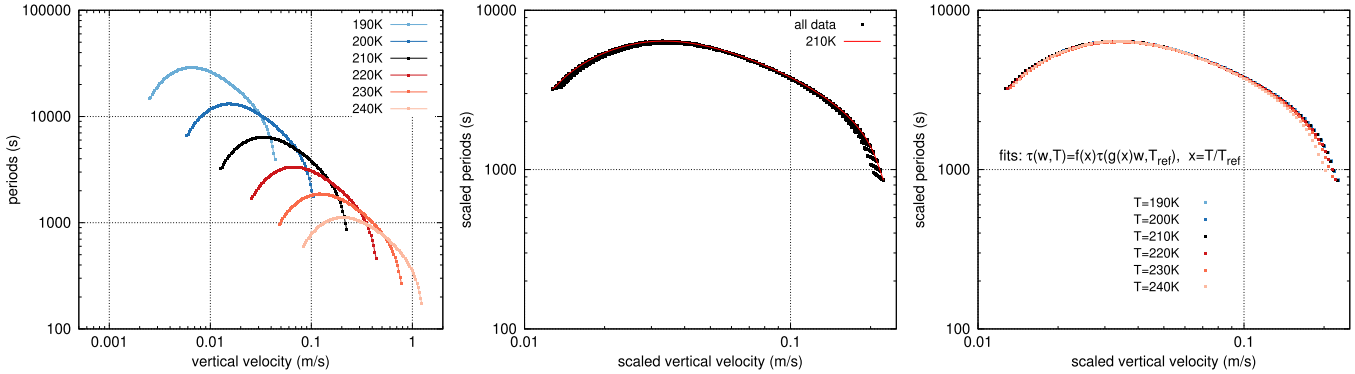

FIG. 7. Scalings of limit cycle's periods. Left: periods of limit cycles for different temperatures; middle: numerical scaling of the data together with the reference curve for $T = 210$ K; right: scaled data using the scaling functions from Eqs. (120) and (121).

the numerically derived periods and calculating shifts for matching the curves, we can map the curves on each other; this is shown in the middle panel of Fig. 7, with the calculated and shifted data as black points and the "reference" period at T_{ref} as a red curve. We can calculate numerically the apparent shifts in position and amplitude, respectively, for the different reduced temperatures x in the temperature interval $190 \le T \le 240$ K, i.e., in the interval $0.9 \le x \le 1.15$. These values are plotted in Fig. 8 as gray dots. Using the expected form for functions $f(x), g(x) \sim x^a$, we find the exponents

$$f(x) = x^{15.0617}, \quad g(x) = x^{-14.1228}; \tag{118}$$

these fits are shown in Fig. 8 as curves in light red or blue. For values $0.95 < x < 1.05$, this approach fits quite well.

However, the scaling functions show deviations to the numerically optimized shift in the data for values x at the boundaries of the interval. Empirically, we find a (much) better fit using the functional form

$$f(x) = x^{a-b(x-1)}, \quad a, b \in \mathbb{R} \text{ Const.}, \tag{119}$$

as indicated in Fig. 8 with curves in dark red or blue. There is small deviation from the fits with a constant scaling exponent, since the functions' coefficients have the following values for f:

$$f(x) = x^{a-b(x-1)}, \quad a = 15.2984, \quad b = 12.013 \tag{120}$$

and for g,

$$g(x) = x^{a-b(x-1)}, \quad a = -14.2715, \quad b = -8.652\,53, \tag{121}$$

respectively. Finally, we apply the adjusted scaling functions $f(x), g(x)$ for matching the periods of different temperatures on each other. As can be seen in the right panel of Fig. 7, this scaling works very well; only at the "boundaries," i.e., for high or low values of x, there are some small deviations, which are probably due to the numerical derivation of the bifurcations. However, we have to state here that the fits are purely empirical, and there is no obvious reason why the periods should have such a scaling behavior. Nevertheless, this is a very interesting property, which in turn also reduces the parameter space for the investigations dramatically. The complete range of bifurcations in the system then boils down to the range of a period determined by just a vertical velocity as shown in the right panel of Fig. 7 for the reference temperature T_{ref} or even the reduced temperature $x = 1$. All other periods in the unstable regime can be derived by the scaling law Eq. (117).

V. COMPARISON TO MEASUREMENTS

In Secs. IV A–IV D, we investigated the qualitative properties of this simplified model. However, the question arises how relevant such a model is in terms of representing ice clouds in the upper troposphere sufficiently well. Thus, we would like to know if the model produces realistic values of the relevant quantities of ice crystal number and mass concentrations. We now compare simulations

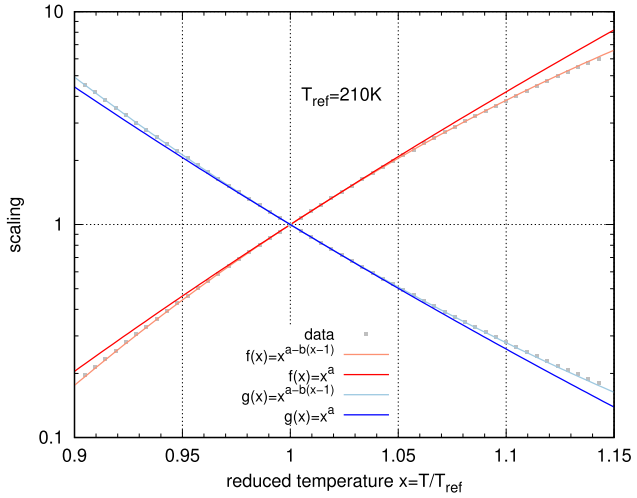

FIG. 8. Fit of exponents of scaling functions. Gray dots: empirical scaling as derived from the numerical calculations. Dark red/blue curves: exponents of the empirical fits using scalings of the functional form $f(x) \sim x^a$, exact values are given in Eq. (118). Light red/blue curves: exponents of the empirical fits using scalings of the functional form $f(x) \sim x^{a-b(x-1)}$, exact values are given in Eqs. (120) and (121).

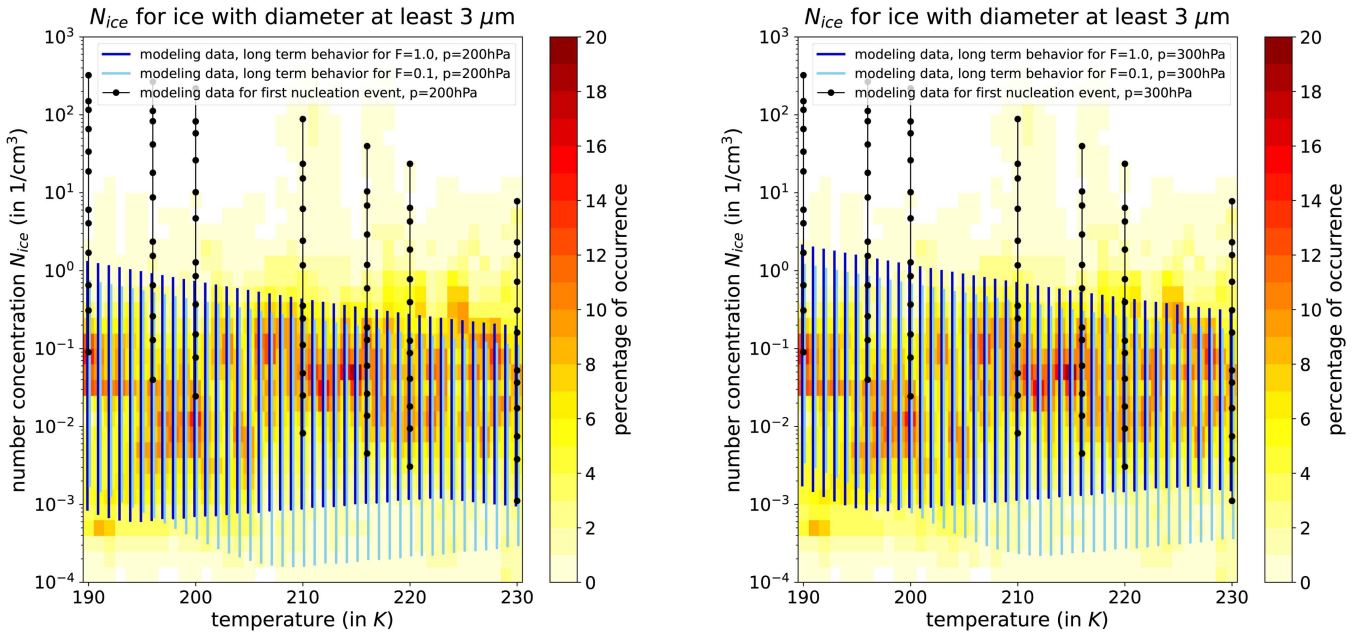

FIG. 9. Comparison of the model results with measurements. Colors indicate the frequency of occurrence of ice crystal number concentrations in measurements.[6,8] Bluish colors show the values of the model, i.e., equilibrium states and range of the limit cycle calculations. Dark blue lines indicate conditions for $F = 1$, light blue indicate conditions for $F = 0.1$, respectively. Black points show undisturbed nucleation events as calculated by Spichtinger *et al.*[22]

of our model with real measurements as obtained from research aircraft, i.e., *in situ* measurements in the tropopause region; these measurements were described in former studies[6,8] and are freely available for scientific evaluations. We use data of ice crystal number concentrations, as obtained from various instruments, which are compiled to a consistent data set.[8] This data set is complied from 24 research campaigns and constitute one of the benchmark data sets for ice cloud research. Since the data are available in units of numbers per volume, we have to recalculate our model values, which are in the conserved variable version of numbers per mass dry air; the conversion is as follows:

$$N|_{\text{per volume}} = \rho \cdot n|_{\text{per mass}}. \tag{122}$$

For this purpose, we have to decide about a given pressure, since the conversion relies on the ideal gas law, thus providing density for given temperature and pressure, respectively. Since most measurements are obtained in the pressure range $200 \leq p \leq 300\,\text{hPa}$, and the model results only weakly depend on the given pressure parameter, we show our results for the two limiting pressure values separately. We compile data for the parameter range of vertical updrafts $0.01 \leq w \leq 2\,\text{m s}^{-1}$, the temperature range $190 \leq T \leq 230\,\text{K}$, two pressure regimes $p = 200, 300\,\text{hPa}$, and two sedimentation regimes $F = 1, 0.1$, respectively. For comparison, we do not indicate full model simulations, but rather the values at the equilibrium points and the ranges of the limit cycles (depending on whether we have a stable equilibrium point or an unstable equilibrium point with limit cycle) as key features of the long term behavior. Moreover, we also include the values of an undisturbed nucleation event as calculated with the model by Spichtinger *et al.*[22]; the temperatures are chosen for comparison with former simulations.[31,50]

In Fig. 9, the comparison of measurements (colors, indicating frequency of occurrence) and model results (blue lines and black linepoints) is displayed. The measurements are sorted in temperature bins of 1 K, the frequency of occurrence is represented by colors. Our model results for the sedimentation factor $F = 1$ are shown in dark blue, whereas light blue indicates results for $F = 0.1$.

We find a good agreement of our model results with the observations. In fact, the qualitative behavior of the model, i.e., equilibrium points and limit cycles, fits very well with the observations. In particular, we want to emphasize that our model simulations are mostly located in the regimes of frequently observed measurements. We see higher values of n for the regime of strong sedimentation $F = 1$, and slightly reduced values for weak sedimentation $F = 0.1$, respectively. Both simulation regimes seem to be reasonable and realistic. The variation due to different pressure regimes is quite marginal, we just see small changes in the picture for different pressure values. In contrast, the values of undisturbed nucleation events in the model are not found in the real observations. The high values at the temperature regime $210 \leq T \leq 220\,\text{K}$ can be attributed to contrails in the measurements.[8] For the higher values of n at higher temperatures, we can assume a different formation mechanism, i.e., liquid origin ice clouds, which are formed by freezing of pre-existing water cloud droplets.[8] Generally, it might be that such high values occur in fresh and undisturbed nucleation events. Nevertheless, it is very hard to observe such events because they are kind of invisible

and now-casting of such events for the aircraft measurements is almost impossible. Overall, the model produces realistic results, as compared to the real measurements. Even the strong simplifications do not crucially affect the results. This makes us confident to use this kind of reduced model for further investigations. Since the model is relatively simple, the analysis is quite easy, but still the model simulations are realistic enough for qualitative and even quantitative behavior of ice clouds in the cold temperature regime. While the parameter space as used in our simple model is quite well represented in the data set, we are quite confident to carry out a robust comparison.

VI. SUMMARY

We develop a simple ice cloud model on the basis of general moments, using number and mass concentrations as cloud variables; in addition, we use the saturation ratio over ice as thermodynamic control variable for driving relevant ice cloud processes such as nucleation and growth of ice particles. The final model consists of a three-dimensional system of nonlinear autonomous ordinary differential equations. The model is then evaluated using the theory of dynamical systems. We show that in the relevant parameter space, there is exactly one equilibrium state. The main feature is here that the problem of finding a root of the vector field can be reformulated to finding a root of a scalar function for the saturation ratio s. The existence and uniqueness of the root are then derived by simple analysis. Furthermore, we can reformulate the scalar function into a sequence generating function and this sequence converges toward the unique fixed point by the Banach fixed point theorem, giving us approximate formulas for the equilibrium states. We also determine the quality of the equilibrium state, using linearization around the equilibrium states and then calculating the respective eigenvalues of the Jacobi matrix numerically. In addition, we prove the existence of a real negative eigenvalue, whereas the other two eigenvalues are either conjugate-complex or both real and negative in the relevant parameter range. The quality of the equilibrium for a variable but fixed temperature T changes with the parameter w (vertical velocity), i.e., switching from a damped oscillation (stable equilibrium) to an undamped oscillation (unstable equilibrium with attracting limit cycle) and back to the damped regime. Thus, we find two supercritical Hopf bifurcations. The bifurcation points in the phase space can be approximated by functions $w(T)$. Using a numerical approach, we derive the periods of the limit cycles in the relevant regime. The range of periods is quite large, producing values between some hundreds of seconds up to several ten thousands of seconds, depending on the environmental conditions. We find a scaling behavior of the bifurcations in terms of the sedimentation parameter F. Using some approximations and properties of the Jacobi matrix, there is a scaling with the square root of F, which can be corroborated by the numerical investigations. Finally, we find an unexpected scaling property for the periods of the limit cycles. Using empirical scaling functions, the periods of limit cycles can be mapped onto a single function, using a reduced temperature scaled by a reference temperature $T_{\mathrm{ref}} = 210\,\mathrm{K}$. The origin of this scaling property is still open.

We compare the qualitative results of the model (i.e., equilibrium states and limit cycle values) with real measurements from aircraft. The model results agree very well with the measurements, placed in the correct region of the parameter space. Hence, we conclude that our very simplified model seems to be able to represent the main features of ice clouds.

VII. CONCLUSION AND OUTLOOK

We have seen that even a quite simplified ice cloud model as a 3D dynamical system can produce realistic cloud states. However, the model is simple enough for theoretical analysis of the general behavior and even for determining important processes and their impact on the time evolution of the system. For instance, we clearly see the importance of the sedimentation as a sink process for the whole system, leading to oscillating behavior. The model might be used for several applications and estimations. For instance, we can estimate the expected values of cloud variables for a certain regime of environmental conditions; this might guide the interpretation of measurements or even help for planning measurements in the upper troposphere, in terms of what cloud regimes we would have to expect. The model can also help to constrain the radiative properties of ice clouds. From values of equilibrium states and potential limit cycles, we could derive estimations of possible optical properties or even robust estimates for the expected radiative impact. The simplest approach would be the calculation of optical depths from the occurring values, similar to former studies.[51,52]

Also, further reduction seems to be an option. Since the analysis showed that the main dynamics take place on a quasi 2D manifold (the contraction in one direction is strong), the resulting behavior might be emulated by a suitable nonlinear oscillator, e.g., a Stuart–Landau oscillator as a normal form of Hopf bifurcations[45] with parameters as derived from the analysis, i.e., prescribing periods from the limit cycle calculations; here, the scaling properties would be very useful. This might result into a reduced order model of ice clouds for coarse resolution models, avoiding, e.g., the parameterization of nucleation processes, which requires quite small time steps.

Beyond the "simple" box model approach of this ice cloud model, we could think of some conceptual extensions. The ice model might be coupled with transport equations or even with mixing terms, similarly to former work,[53] to a spatial extension, leading to reaction–diffusion equations, which can be analyzed in terms of possible structure formation such as, e.g., Turing instabilities.[54] Since the model is well characterized as an ODE system, linearization or even the use of weakly nonlinear theory might lead to conceptual understanding of potential emergence of structures.

Our bulk approach turned out to be very robust. However, it is not really clear if the same kind of robust physical behavior can be observed in conceptually different models, as, e.g., based on the full Boltzmann-type evolution equation. Qualitative comparison of these different model approaches would also lead to a better understanding of the representation of cloud structures on different scales.

Finally, we can think of a robust application of the derived properties of the model for the real world. The values of equilibrium states as well as the spread of the cloud variables in the limit cycles could be used as good estimates for measurements at different platforms. The periods of the limit cycles might translate into

spatial pattern in clouds as might be seen from satellites, e.g., from the new EarthCare products dedicated for cloud research. Thus, the theoretical investigations of a reduced order model might help to understand real measurements and properties of ice clouds.

ACKNOWLEDGMENTS

We thank the reviewers for important comments, which lead to a significant improvement of the manuscript. We acknowledge support by the Deutsche Forschungsgemeinschaft (DFG) within the Transregional Collaborative Research Centre TRR301 TPChange (Project-ID 428312742), project B7. We thank Martina Krämer for some discussions about ice crystal measurements. We thank Philipp Reutter for help with plotting. We thank Friederike Schmid for the helpful comment about deriving scaling laws from logarithmic plots. P.S. thanks Eberhard Bodenschatz for his hospitality at MPI-DS, where parts of this article were written.

AUTHOR DECLARATIONS

Conflict of Interest

The authors have no conflicts to disclose.

Author Contributions

P.S. developed the simple model, H.B. and P.S. carried out the mathematical analysis, H.B. carried out the comparison with measurements. Both authors wrote together the manuscript.

Hannah Bergner: Conceptualization (equal); Investigation (equal); Writing – original draft (equal). **Peter Spichtinger:** Conceptualization (equal); Methodology (equal); Writing – original draft (equal).

DATA AVAILABILITY

The data produced by the respective model that support the findings of this study are partly available within the article and also available from the corresponding author upon reasonable request. In addition, the data for model comparison are openly available in B2SHARE at https://doi.org/10.34730/266ca2a41f4946ff97d874bfa458254c, Ref. 55.

APPENDIX A: DERIVATION OF THE MODEL EQUATIONS

1. Moment equations

We start with the general Boltzmann equation for the mass distribution $f(m,t,x)$; in the following we will suppress the dependency on (t,x) in the notation. The equation

$$\frac{\partial \rho f}{\partial t} + \nabla \cdot (\rho f u) + \frac{\partial (\rho f g)}{\partial m} = \rho h \tag{A1}$$

is equipped with a 3D fluid velocity v and a terminal velocity of particles v_t relative to the center of gravity of the flow, i.e., $u = v - e_z v_t$, thus we find

$$\frac{\partial \rho f}{\partial t} + \nabla \cdot (\rho f v) - \frac{\partial}{\partial z}(\rho f v_t) + \frac{\partial}{\partial m}(\rho f g) = \rho h. \tag{A2}$$

Using the continuity equation $\rho_t + \nabla \cdot (\rho v) = 0$, we can reformulate the Boltzmann equation in a more convenient form

$$\frac{\partial f}{\partial t} + v \cdot \nabla f + \frac{\partial}{\partial m}(fg) = \frac{1}{\rho}\frac{\partial (\rho f v_t)}{\partial z} + h, \tag{A3}$$

where we set $\dot{m} = g$ in a more suggestive notation. Now, we multiply the whole equation by powers of the mass coordinate m^k, thus,

$$\frac{\partial}{\partial t}(m^k f) + v \cdot \nabla (m^k f) + m^k \frac{\partial}{\partial m}(\dot{m} f) = \frac{1}{\rho}\frac{\partial}{\partial z}\left(\rho m^k f v_t\right) + m^k h. \tag{A4}$$

Now, all terms are integrated over the whole mass range $(0,\infty)$. For the first two terms, we directly obtain the general moments, i.e.,

$$\int_0^\infty \left(\frac{\partial}{\partial t}\left(m^k f\right) + v \cdot \nabla\left(m^k f\right)\right) \mathrm{d}m = \frac{\partial \mu_k}{\partial t} + v \cdot \nabla(\mu_k), \tag{A5}$$

in case of convergence of the integrals. For the growth term, we have to treat different cases. First, we investigate the case $k \in \mathbb{N}$. Then, we can use partial integration in order to obtain

$$\int_0^\infty m^k \frac{\partial}{\partial m}(\dot{m} f)\mathrm{d}m = m^k \dot{m} f(m)\Big|_0^\infty - k\int_0^\infty m^{k-1}\dot{m} f \mathrm{d}m. \tag{A6}$$

For the convergence of the integrals, we have to assume boundary conditions

$$\lim_{m\to\infty} m^\alpha f(m) = 0 \;\forall \alpha \in \mathbb{R}_+ \quad \text{and} \quad \lim_{m\to 0} \dot{m} f(m) < \infty, \tag{A7}$$

thus, we obtain

$$\int_0^\infty m^k \frac{\partial}{\partial m}(\dot{m} f)\mathrm{d}m = -k\int_0^\infty m^{k-1}\dot{m} f \mathrm{d}m. \tag{A8}$$

This is the growth and evaporation rate for all moments $k \geq 1$. For $k = 0$ (i.e., in case of the number concentration), we find

$$\int_0^\infty \frac{\partial}{\partial m}(\dot{m} f)\mathrm{d}m = \dot{m} f(m)\Big|_0^\infty = -\dot{m} f(0), \tag{A9}$$

which is the evaporation rate of the system. Obviously, it strongly depends on the distribution f and not on its moments. This investigation is subject of future research. For the remaining two terms on the right-hand side (sedimentation/sources), there is no general simplification possible, we will treat sedimentation in Appendix A 5.

2. Nucleation for ensemble of solution droplets

The amount of newly nucleated ice particles from a distribution of solution droplets $f(r)$ can be derived as follows. Starting with the probability for freezing a particle of volume V within a time interval Δt, i.e.,

$$P = 1 - \exp(-JV\Delta t), \tag{A10}$$

we determine the difference of newly nucleated particles as

$$\Delta n = \int_0^\infty f(r)P(r)\mathrm{d}r = \int_0^\infty f(r)(1 - \exp(-JV\Delta t))\mathrm{d}r. \tag{A11}$$

Using an expansion in the small time interval (assuming $\frac{\partial J}{\partial r} = 0$), we obtain

$$\begin{aligned}\Delta n = \int_0^\infty f(r)P(r)\mathrm{d}r &= \int_0^\infty f(r)\left(1-\left(1-JV\Delta t+\mathcal{O}\left(\Delta t^2\right)\right)\right)\mathrm{d}r \\ &= \int_0^\infty f(r)JV\mathrm{d}r\cdot\Delta t+\mathcal{O}\left(\Delta t^2\right) \\ &= J\frac{4}{3}\pi\int_0^\infty f(r)r^3\mathrm{d}r\cdot\Delta t+\mathcal{O}\left(\Delta t^2\right) \\ &= J\frac{4}{3}\pi\mu_3[m]\cdot\Delta t+\mathcal{O}\left(\Delta t^2\right) \end{aligned} \tag{A12}$$

and after dividing by Δt and obtaining the limit $\Delta t \to 0$, we find

$$\frac{\mathrm{d}n}{\mathrm{d}t} = J\frac{4}{3}\pi\mu_3[m], \tag{A13}$$

with the general third moment of the underlying size distribution of the solution droplets. As in former investigations,[31] we use a lognormal distribution for the radius of aqueous solution droplets of the form

$$f_a(r) = \frac{n_a}{\sqrt{2\pi}\log(\sigma_r)r}\exp\left(-\frac{1}{2}\left(\frac{\log\left(\frac{r}{r_m}\right)}{\log(\sigma_r)}\right)^2\right), \tag{A14}$$

with the modal radius $r_m = r_{\mathrm{sol}}$ of the distribution (i.e., the modal radius of solution droplets). Since we do not explicitly treat the aerosol properties, we make the assumptions that (a) the type and size of the aerosol does not change and (b) the amount of nucleated ice crystals is always several orders smaller than the aerosol concentration n_a, thus n_a remains constant. According to the investigations by Spichtinger and Gierens,[31] we specify $r_m = r_{\mathrm{sol}} = 75\times10^{-9}\,\mathrm{m}$ and the geometric standard deviation $\sigma_r = 1.5$. Using the analytical description of general moments, we can derive the mean volume of a solution droplet as

$$V_{\mathrm{sol}} = \frac{4}{3}\pi r_{\mathrm{sol}}^3\cdot c_{\mathrm{sol}},\quad c_{\mathrm{sol}} = \exp\left(\frac{9}{2}\left(\log\sigma_r\right)^2\right). \tag{A15}$$

The typical mass of a freshly nucleated ice particle can be set to $m_{\mathrm{nuc}} = 10^{-16}\,\mathrm{kg}$. Finally, we can assume a typical concentration of solution droplets in the upper troposphere in order of $N_a \sim 300\,\mathrm{cm}^{-3} = 3\times10^8\,\mathrm{m}^{-3}$. Using the density ρ as obtained by the ideal gas law from temperature and pressure, we can determine $n_a = \frac{N_a}{\rho}$.

Remark: For comparison with the reference values as determined by Kärcher and Lohmann,[50] we often use an unrealistically high aerosol number concentration $N_a = 10\,000\,\mathrm{cm}^{-3}$. Note that the resulting scaling of the nucleation term only marginally affects the nucleation events.[22]

In summary, the nucleation term for the number concentration can be expressed as

$$\mathrm{Nuc}_n = \left.\frac{\partial n}{\partial t}\right|_{\mathrm{nucleation}} = n_a V_{\mathrm{sol}} J. \tag{A16}$$

For the mass concentration rate Nuc_q, we multiply Nuc_n by the constant mass m_{nuc}. The nucleation rate is determined[22] by

$$J(s,T) = J_0\exp(p_{1\mathrm{e}}(T)(s-p_2(T))),\quad J_0 = 10^{16}\,\mathrm{m}^{-3}\,\mathrm{s}^{-1} \tag{A17}$$

and polynomials

$$p_1(T) = a_0 + a_1 T,\quad p_{1\mathrm{e}}(T) = \log(10)p_1(T), \tag{A18}$$

$$p_2(T) = a_{s2}T^2 + a_{s1}T + a_{s0}, \tag{A19}$$

with coefficients

$$a_0 = -50.4085,\quad a_1 = 0.9368\,\mathrm{K}^{-1} \tag{A20}$$

and

$$a_{s2} = -1.369\,89\times10^{-5}\,\mathrm{K}^{-2}, \tag{A21}$$

$$a_{s1} = 0.002\,28\,\mathrm{K}^{-1},\quad a_{s0} = 1.674\,69. \tag{A22}$$

3. Parameters and functions

The ideal gas constants are given by

$$R_d \approx 287.058\,\mathrm{J\,kg^{-1}\,K^{-1}},\quad R_v \approx 461.553\,\mathrm{J\,kg^{-1}\,K^{-1}}, \tag{A23}$$

the acceleration by gravity is determined as $g = 9.81\,\mathrm{m/s^2}$. For the latent heat of sublimation, we use the formulation by Murphy and Koop[24]

$$L(T) = L_{\mathrm{mol}}(T)/M_{\mathrm{mol},v}, \tag{A24}$$

$$L_{\mathrm{mol}}(T) = l_0 + l_1 T + l_2 T^2 + l_3\exp\left(-(T/T_l)^2\right), \tag{A25}$$

with coefficients

$$l_0 = 46\,782.5\,\mathrm{J\,mol^{-1}},\quad l_1 = 35.8925\,\mathrm{J\,mol^{-1}\,K^{-1}}, \tag{A26}$$

$$l_2 = -0.074\,14\,\mathrm{J\,mol^{-1}\,K^{-2}},\quad l_3 = 541.5\,\mathrm{J\,mol^{-1}}, \tag{A27}$$

$$T_l = 123.75\,\mathrm{K}, \tag{A28}$$

$$M_{\mathrm{mol},v} = 18.015\,28\times10^{-3}\,\mathrm{kg\,mol^{-1}}. \tag{A29}$$

The saturation vapor pressure over hexagonal ice[24] is expressed as

$$p_{\mathrm{si}}(T) = p_{\mathrm{unit}}\exp(b_0 + b_1/T + b_2\log(T/T_{\mathrm{unit}}) + b_3 T), \tag{A30}$$

with

$$p_{\mathrm{unit}} = \mathrm{Pa},\quad T_{\mathrm{unit}} = \mathrm{K} \tag{A31}$$

and

$$b_0 = 9.550\,426,\quad b_1 = -5723.265\,\mathrm{K}, \tag{A32}$$

$$b_2 = 3.530\,68,\quad b_3 = -0.007\,283\,32\,\mathrm{K}^{-1}. \tag{A33}$$

The heat conduction of air[37] is given by

$$K_T(T) = \frac{a_K T^{b_K}}{T + T_K\cdot10^{\frac{c_K}{T}}}, \tag{A34}$$

with coefficients

$$a_K = 0.002\,646\,\mathrm{W\,m^{-1}\,K^{1-b_K}}, \quad b_K = \frac{3}{2}, \tag{A35}$$

$$T_K = 245\,\mathrm{K}, \quad c_K = -12\,\mathrm{K}. \tag{A36}$$

4. Growth for an ensemble of spherical ice particles

Using the description of the mass growth rate for a single particle of mass m, i.e.,

$$\dot{m} = 4\pi C D_v f_k G_v (s-1) f_v, \tag{A37}$$

the averaged growth rate for the first moment, i.e., the mass concentration $q = \mu_1[m]$, is then given by

$$\mathrm{Dep}_q = \int_0^\infty \dot{m} f(m)\mathrm{d}m = \int_0^\infty 4\pi C D_v f_k G_v (s-1) f_v f(m)\mathrm{d}m. \tag{A38}$$

We now apply several simplifications for deriving a simplified version of the growth rate. We neglect the corrections for the kinetic regime ($f_k = 1$) and for ventilation ($f_v = 1$). In addition, we assume spherical particles, which, in turn, leads to a capacity factor $C(m) = r = c\,m^{\frac{1}{3}}$ [see Eq. (31)]. Finally, we fix the type of the mass distribution as a lognormal distribution [see Eq. (34)], thus we can use the analytical description of the general moments. This leads to the following representation of the growth term as:

$$\begin{aligned}
\mathrm{Dep}_q &= \int_0^\infty f(m) 4\pi C D_v f_k G_v (s-1) f_v \,\mathrm{d}m \\
&\approx 4\pi G_v D_v \int_0^\infty f(m) C(m)\mathrm{d}m \cdot (s-1) \\
&= 4\pi G_v D_v\, c\, r_0^{-\frac{1}{9}} n^{\frac{2}{3}} q^{\frac{1}{3}} (s-1) \\
&= B_q n^{\frac{2}{3}} q^{\frac{1}{3}} (s-1),
\end{aligned} \tag{A39}$$

where

$$B_q = 4\pi G_v D_v c r_0^{-\frac{1}{9}}, \tag{A40}$$

with G_v as in Eq. (50), D_v as in Eq. (47), and $c = \sqrt[3]{\frac{3}{4\pi\rho_b}}$ as in Eq. (31). The use of $f_k = 1$ is motivated in Appendix A 6.

5. Sedimentation for an ensemble of particles

For the sedimentation of the averaged quantities, we rewrite the sedimentation part in terms of a transport equation. We investigate the vertical sedimentation flux of a quantity ψ (i.e., a general moment μ_k), i.e., $j_\psi = \rho\psi v_\psi$ with the respective vertical velocity v_ψ, thus the advection equation can be written as

$$\frac{\partial(\rho\psi)}{\partial t} = \frac{\partial j_\psi}{\partial z}. \tag{A41}$$

For the averaged variables $n = \mu_0, q = \mu_1$, we define the fluxes as

$$j_n := \int_0^\infty \rho f(m) v_t(m)\mathrm{d}m \stackrel{!}{=} \rho n v_n, \tag{A42}$$

$$j_q := \int_0^\infty \rho f(m) m v_t(m)\mathrm{d}m \stackrel{!}{=} \rho q v_q \tag{A43}$$

expressed by averaged velocities

$$v_n = \frac{1}{n}\int_0^\infty f(m) v_t(m)\mathrm{d}m, \tag{A44}$$

$$v_q = \frac{1}{q}\int_0^\infty f(m) m v_t(m)\mathrm{d}m. \tag{A45}$$

Note that from the formulation of the sedimentation as a transport equation, it is obvious that for positive quantities n, q in the time evolution, they will never take a value $= 0$.

6. Approximations

In Eq. (30), we make the approximation

$$\frac{L^2}{c_p R_v T^2} S_i + \frac{p}{\varepsilon p_{\mathrm{si}}} \approx \frac{p}{\varepsilon p_{\mathrm{si}}}, \tag{A46}$$

a short calculation shows that the first term contributes less than 20% at the warmest temperature $T = 240$ K, whereas for temperatures lower than 230 K (respectively, 210 K), the contribution is less than 10% (respectively, 1%).

For the growth equation of a single ice crystal, we omit the kinetic correction, i.e., we set $f_k = 1$. As can be seen in the top panel of Fig. 10, the kinetic correction is most active for very small ice crystals, and this is most relevant for modeling ice nucleation in cloud free air at cold temperatures with high vertical updrafts[22,31]; freshly nucleated ice crystals are very small (radius about 1 μm) and the growth is dominated by the kinetic regime. The correction guarantees that the nucleation is not turned off too early by the ice crystals' growth, reducing the supersaturation. For scenarios as in our "long term" simulations, the ice crystals never disappear, and the mean mass of ice crystals stays at larger values. Thus, the kinetic correction is not relevant. We evaluated our simulations afterwards, and we observed the largest spread in mean mass or size for limit cycle scenarios. However, even for the lowest temperature 190 K, the mass was always larger than $m \sim 10^{-13}$ kg (except for the very first nucleation event). For higher temperatures the mass was usually larger than $m \sim 10^{-12}$ kg; thus even from a backward perspective, neglecting the kinetic correction is justified.

In the formulation of the terminal velocity of ice crystals, we made the approximation

$$v_{\mathrm{final}} a_s m^{b_s} \frac{1}{v_{\mathrm{final}} + a_s m^{b_s}} \approx a_s m^{b_s}. \tag{A47}$$

As can be seen in the bottom panel of Fig. 10, the deviation is only relevant for large particles. From real measurements[6] we obtain that the radius of ice crystals is smaller than $r \sim 100\,\mu$m, and actually the radius stays below $r \sim 80\,\mu$m. Thus, from a measurement viewpoint, the *a priori* approximation is meaningful since the deviation is less than 25%. From the evaluation of our simulations, with the largest spread in the limit cycle scenarios, we find that the mean radius is less than $r \sim 67\,\mu$m for simulations at $T = 240$ K, and even smaller for lower temperatures. Thus, the approximation can also be justified from the backward perspective.

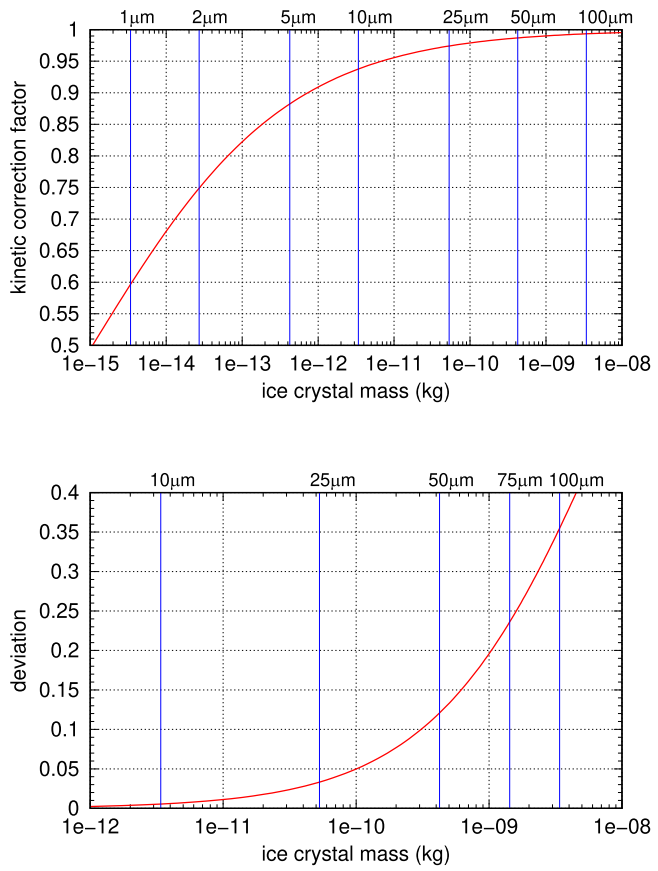

FIG. 10. Impact of kinetic correction factor (top panel), and deviation from correct terminal velocity (bottom panel).

APPENDIX B: EQUILIBRIUM STATES OF THE ICE CLOUD MODEL

In this section, we first show that the terms Nuc_q and Nuc_s are very small compared to the other terms of the ODE system close to an equilibrium point and can, hence, be neglected to a good approximation when determining the equilibrium points of the system. Then, we present the calculations for the derivation of the scalar function $f(x)$ as defined in Eq. (75) whose roots are in one-to-one correspondence with the equilibrium points of the system.

1. Estimates for the nucleation terms Nuc_q and Nuc_s near the equilibrium point

In the following, we prove that the terms Nuc_q and Nuc_s are very small in the vicinity of equilibrium points of the system and hence, a very good approximation of the equilibrium points can be found while neglecting these terms.

First, observe that

$$n^{\frac{2}{3}} q^{\frac{1}{3}} = n\bar{m}^{\frac{1}{3}}, \quad n^{\frac{1}{3}} q^{\frac{2}{3}} = n\bar{m}^{\frac{2}{3}}, \tag{B1}$$

where $\bar{m} = \frac{q}{n}$ denotes the mean mass of ice crystals. We are interested in the supersaturated regime where $s > 1$ and thus $\mathrm{Evap}_n = 0$. Since $\frac{dn}{dt} = 0$ at an equilibrium point, we get

$$A_n \exp(p_{1e}(s - p_2)) = FC_n n\bar{m}^{\frac{2}{3}} = r_0^{-\frac{2}{3}} FC_q n\bar{m}^{\frac{2}{3}} \tag{B2}$$

from Eq. (4), where we also used $C_n = r_0^{-\frac{2}{3}} C_q$. Therefore, we further have

$$\mathrm{Nuc}_q = m_{\mathrm{nuc}} A_n \exp(p_{1e}(s - p_2)) \tag{B3}$$

$$= m_{\mathrm{nuc}} r_0^{-\frac{2}{3}} FC_q n\bar{m}^{\frac{2}{3}} = -\frac{m_{\mathrm{nuc}} r_0^{-\frac{2}{3}}}{\bar{m}} \mathrm{Sed}_q, \tag{B4}$$

since $\mathrm{Nuc}_q = m_{nuc}\mathrm{Nuc}_n$ with $m_{\mathrm{nuc}} = 10^{-16}$ kg as the typical mass of a newly nucleated ice crystal. Using Eq. (2), the condition of $\frac{dq}{dt} = 0$ at an equilibrium point then translates into

$$0 = \mathrm{Dep}_q + \mathrm{Nuc}_q + \mathrm{Sed}_q \tag{B5}$$

$$= \mathrm{Dep}_q + (1 - \delta)\mathrm{Sed}_q, \tag{B6}$$

for $\delta := \frac{m_{\mathrm{nuc}} r_0^{-\frac{2}{3}}}{\bar{m}}$, and since $r_0^{-\frac{2}{3}} < 1$ (because $r_0 > 1$ by definition), we see that we can neglect the term Nuc_q up to a good approximation if the mean mass $\bar{m}$ at the equilibrium point satisfies $\bar{m} \gg m_{\mathrm{nuc}}$.

Moreover, using the above and the definitions of Nuc_s, Dep_s as in Eqs. (45) and (53), we also get

$$\mathrm{Nuc}_s = -\frac{p}{\varepsilon p_{\mathrm{si}}} \mathrm{Nuc}_q = \frac{p}{\varepsilon p_{\mathrm{si}}} \delta \cdot \mathrm{Sed}_q \tag{B7}$$

$$= -\frac{p}{\varepsilon p_{\mathrm{si}}} \frac{\delta}{1 - \delta} \mathrm{Dep}_q = \frac{\delta}{1 - \delta} \mathrm{Dep}_s. \tag{B8}$$

The condition of $\frac{ds}{dt} = 0$ at the equilibrium point then translates by Eq. (3) into

$$0 = \mathrm{Cool} + \mathrm{Nuc}_s + \mathrm{Dep}_s \tag{B9}$$

$$= \mathrm{Cool} + \left(\frac{\delta}{1 - \delta} + 1 \right) \mathrm{Dep}_s \tag{B10}$$

$$= \mathrm{Cool} + \frac{1}{1 - \delta} \mathrm{Dep}_s, \tag{B11}$$

and it turns out that also the term Nuc_s can be neglected up to a good approximation if $\bar{m} \gg m_{\mathrm{nuc}}$ (and thus $\delta \ll 1$) at the equilibrium point.

It remains to show that the mean mass $\bar{m}$ satisfies $\bar{m} \gg m_{\mathrm{nuc}}$ near an arbitrary equilibrium state of the system. This can be done by distinguishing two cases for the value of $s \geq 1$ at the equilibrium point, first, the case where s is close to 1, and second, the case where s is larger.

First, assume $s \leq 1.35$ at the equilibrium point. Since $\frac{dn}{dt} = 0$ and we are in the supersaturated regime with $s \geq 1$, we have at the

equilibrium point

$$Dw \le Dw\, s = \mathrm{Cool} = -(\mathrm{Nuc}_s + \mathrm{Dep}_s) \tag{B12}$$

$$= \frac{p}{\varepsilon p_{\mathrm{si}}}(\mathrm{Nuc}_q + \mathrm{Dep}_q) = -\frac{p}{\varepsilon p_{\mathrm{si}}}\mathrm{Sed}_q \tag{B13}$$

$$= \frac{p}{\varepsilon p_{\mathrm{si}}} FC_q n \bar{m}^{\frac{5}{3}} = -\frac{p}{\varepsilon p_{\mathrm{si}}} \bar{m} r_0^{\frac{2}{3}} \mathrm{Sed}_n \tag{B14}$$

$$= \frac{p}{\varepsilon p_{\mathrm{si}}} \bar{m} r_0^{\frac{2}{3}} \mathrm{Nuc}_n \tag{B15}$$

$$= \frac{p}{\varepsilon p_{\mathrm{si}}} \bar{m} r_0^{\frac{2}{3}} A_n \exp(p_{1\mathrm{e}}(s - p_2)) \tag{B16}$$

$$\le \frac{p}{\varepsilon p_{\mathrm{si}}} \bar{m} r_0^{\frac{2}{3}} A_n \exp(p_{1\mathrm{e}}(1.35 - p_2)), \tag{B17}$$

where we also use $\mathrm{Nuc}_q + \mathrm{Dep}_q = -\mathrm{Sed}_q$ and $\mathrm{Sed}_n = -\mathrm{Nuc}_n$ due to $\frac{dq}{dt} = 0$ and $\frac{dn}{dt} = 0$, and in $s \le 1.35$ in the last step. Therefore, we get the following estimate for the mean mass $\bar{m}$ at the equilibrium point:

$$\bar{m} \ge \frac{Dw}{A_n} \frac{\varepsilon p_{\mathrm{si}}}{p} r_0^{-\frac{2}{3}} \exp(-p_{1\mathrm{e}}(1.35 - p_2)) \tag{B18}$$

$$\ge \frac{Dw_{\min}}{A_n} \frac{\varepsilon p_{\mathrm{si}}}{p} r_0^{-\frac{2}{3}} \exp(-p_{1\mathrm{e}}(1.35 - p_2)), \tag{B19}$$

where $w_{\min} = 0.0005\,\mathrm{m\,s^{-1}}$ is the minimal vertical velocity we consider (cf., Table I). Calculating the terms in Eq. (B19) for different temperatures/pressures yields that its minimal possible values for the ranges as in Table I is larger that 10^{-2} kg, and thus, we get for the mean mass at the equilibrium point

$$\bar{m} \ge 10^{-2}\,\mathrm{kg} \gg m_{\mathrm{nuc}} = 10^{-16}\,\mathrm{kg} \tag{B20}$$

as desired. (Note here, that this first case with the assumption of $s \le 1.35$ at the equilibrium point yields physically unrealistically heavy/large ice crystals, and it becomes clear from further investigation in Sec. IV A that the case with $s \le 1.35$ at an equilibrium point does not appear.)

Second, we now consider the case of an equilibrium point with $s \ge 1.35$. From $\frac{dq}{dt} = 0$, $\mathrm{Sed}_q < 0$, and $F \le 1$, we get

$$B_q n \bar{m}^{\frac{1}{3}}(s - 1) = \mathrm{Dep}_q = -(1 - \delta)\mathrm{Sed}_q \tag{B21}$$

$$\le -\mathrm{Sed}_q = FC_q n \bar{m}^{\frac{5}{3}} \le C_q n \bar{m}^{\frac{5}{3}}, \tag{B22}$$

and hence, using $s \ge 1.35$,

$$B_q(1.35 - 1) \le B_q(s - 1) \le C_q \bar{m}^{\frac{4}{3}} \tag{B23}$$

$$\Leftrightarrow\ \bar{m} \ge \left(\frac{B_q}{C_q}(1.35 - 1)\right)^{\frac{3}{4}}. \tag{B24}$$

A calculation of this with the explicit forms for B_q, C_q for different temperatures/pressures in the ranges as specified in Table I, then results in

$$\bar{m} \ge \left(\frac{B_q}{C_q}(1.35 - 1)\right)^{\frac{3}{4}} \ge 10^{-12}\,\mathrm{kg} \gg m_{\mathrm{nuc}} = 10^{-16}\,\mathrm{kg}. \tag{B25}$$

Consequently, we indeed have $\bar{m} \gg m_{\mathrm{nuc}}$ for the mean mass $\bar{m}$ of ice crystals at an arbitrary equilibrium point and by the above arguments this implies that we may neglect the terms Nuc_q and Nuc_s up to a very good approximation when determining the equilibrium points of the system.

2. Derivation of the scalar function for the equilibrium states

We now derive the scalar function $f(x)$ as defined in Eq. (75) whose roots are in one-to-one correspondence with the equilibrium points of the system. In fact, the roots of $f(x)$ are precisely the values s_0 of the supersaturation at an equilibrium point and the values of the number and mass concentrations at the equilibrium point can be uniquely calculated from s_0.

We use the condition for the equilibrium state (i.e., $\frac{\mathrm{d}\psi}{\mathrm{d}t} = 0$) for deriving expressions for n and $\bar{m}$. We start with the equation for n,

$$A_n \exp(p_{1\mathrm{e}}(s - p_2)) - FC_n n^{\frac{1}{3}} q^{\frac{2}{3}} = 0 \tag{B26}$$

$$\Leftrightarrow\ A_n \exp(p_{1\mathrm{e}}(s - p_2)) = FC_n n \bar{m}^{\frac{2}{3}} \tag{B27}$$

$$\Leftrightarrow\ n = \frac{A_n}{FC_n} \exp(p_{1\mathrm{e}}(s - p_2)) \bar{m}^{-\frac{2}{3}}. \tag{B28}$$

Then, we find an expression for $\bar{m}$ by dividing Eq. (73) by $q \ne 0$,

$$B_q n^{\frac{2}{3}} q^{-\frac{2}{3}}(s - 1) - FC_q n^{-\frac{2}{3}} q^{\frac{2}{3}} = 0 \tag{B29}$$

$$\Leftrightarrow\ B_q \bar{m}^{-\frac{2}{3}}(s - 1) = FC_q \bar{m}^{\frac{2}{3}} \tag{B30}$$

$$\Leftrightarrow\ B_q(s - 1) = FC_q \bar{m}^{\frac{4}{3}} \tag{B31}$$

$$\Leftrightarrow\ \bar{m}^{\frac{4}{3}} = \frac{B_q}{FC_q}(s - 1) \tag{B32}$$

$$\Leftrightarrow\ \bar{m} = \left(\frac{B_q}{FC_q}(s - 1)\right)^{\frac{3}{4}}. \tag{B33}$$

This produces the equations for the values of n, q at the equilibrium state

$$n = \frac{A_n}{FC_n} \exp(p_{1\mathrm{e}}(s - p_2)) \left(\frac{B_q}{FC_q}(s - 1)\right)^{-\frac{1}{2}} \tag{B34}$$

and

$$q = n\bar{m} = \frac{A_n}{FC_n} \exp(p_{1\mathrm{e}}(s - p_2)) \left(\frac{B_q}{FC_q}(s - 1)\right)^{\frac{1}{4}}. \tag{B35}$$

The value of the saturation ratio at the equilibrium state can be obtained by

$$Dw\, s - B_s n \bar{m}^{\frac{1}{3}}(s - 1) = 0 \Leftrightarrow \tag{B36}$$

$$Dw\,s - B_s \frac{A_n}{FC_n} \exp(p_{1e}(s-p_2)) \left(\frac{B_q}{FC_q}(s-1)\right)^{-\frac{1}{4}} (s-1) = 0. \tag{B37}$$

This last equation is used for the definition of the scalar function $f(x)$ for $x = s$, i.e.,

$$f(x) = ax - \frac{b\,(x-1)\exp(c\,(x-x_0))}{\sqrt[4]{d\,(x-1)}}, \tag{B38}$$

with the coefficients

$$a = Dw, \quad b = B_s \frac{A_n}{FC_n}, \quad c = p_{1e}, \quad d = \frac{B_q}{FC_q}, \quad x_0 = p_2. \tag{B39}$$

Rearranging the equation and the coefficients leads to the definition of $f(x)$ as in Eq. (75) and if s_0 is the supersaturation at any equilibrium point of the ODE system, it satisfies $f(s_0) = 0$. Vice versa, given an arbitrary root s_0 of the function $f(x)$, we set the number concentration n_0 and mass concentration q_0 to be given by Eqs. (B34) and (B35) for $s = s_0$; then, $x = (n_0, q_0, s_0)^T$ is an equilibrium point of the ODE system, which can be verified by a short calculation.

APPENDIX C: ESTIMATES FOR THE CONTRACTION

In the following, we show that the function $h(x)$ as defined in Eq. (85) satisfies

$$h([s_{\min}, s_{\max}]) \subset [s_{\min}, s_{\max}] \tag{C1}$$

for $s_{\min} = 1.37$ and $s_{\max} = 1.59$. First, we estimate the ranges of functions σ and p_{1e}, respectively. For the relevant ranges of temperature ($190 \le T \le 240$ K) and pressure ($200 \le p \le 300$ hPa), we find

$$\sigma_1 \le \sigma \le \sigma_2, \quad \pi_1 \le \frac{1}{p_{1e}(T)} \le \pi_2 \tag{C2}$$

for parameters

$$\sigma_1 = 1.412\,801, \quad \sigma_2 = 1.583\,606, \tag{C3}$$

$$\pi_1 = 0.002\,489, \quad \pi_2 = 0.003\,404. \tag{C4}$$

Next, we would like to estimate the term

$$\gamma_1 \le \frac{1}{p_{1e}} \left(\log(w) + \frac{3}{4}\log(F)\right) \le \gamma_2 \tag{C5}$$

by lower and upper bounds γ_1, γ_2 for the relevant ranges

$$0.01 = F_{\min} \le F \le F_{\max} = 1, \tag{C6}$$

$$0.0005\ \mathrm{m\,s^{-1}} = w_{\min} \le w \le w_{\max} = 2\ \mathrm{m\,s^{-1}}. \tag{C7}$$

Therefore, we set

$$\gamma_2 = 0.002\,360 \ge \pi_2 \left(\log(w_{\max}) + \frac{3}{4}\log(F_{\max})\right), \tag{C8}$$

$$\gamma_1 = -0.037\,631 \le \pi_2 \left(\log(w_{\min}) + \frac{3}{4}\log(F_{\min})\right), \tag{C9}$$

which then satisfy Eq. (C5). Thus, we find the estimation

$$\begin{aligned} 1.375\,170 = \sigma_1 + \gamma_1 &\le \sigma + \frac{1}{p_{1e}} \left(\log(w) + \frac{3}{4}\log(F)\right) \\ &\le \sigma_2 + \gamma_2 = 1.585\,966, \end{aligned} \tag{C10}$$

and hence, get

$$h(x) = \kappa_0 + \frac{1}{p_{1e}} \log\left(\frac{x}{(x-1)^{\frac{3}{4}}}\right) \tag{C11}$$

for some (variable) $\kappa_0 \in [1.375\,170, 1.585\,966]$. Let us now specify the following interval:

$$[s_{\min}, s_{\max}] \quad \text{with } s_{\min} = 1.37, \quad s_{\max} = 1.59. \tag{C12}$$

Calculating all possible values of $\log\left(\frac{x}{(x-1)^{\frac{3}{4}}}\right)$ on the interval $[s_{\min}, s_{\max}]$, we obtain

$$0.002\,139 \le \frac{1}{p_{1e}} \log\left(\frac{x}{(x-1)^{\frac{3}{4}}}\right) \le 0.003\,670 \tag{C13}$$

such that

$$\begin{aligned} h([s_{\min}, s_{\max}]) &\subset [1.375\,170, 1.585\,966] + [0.002\,139, 0.003\,670] \\ &= [1.377\,309, 1.589\,636] \subset [s_{\min}, s_{\max}]. \end{aligned} \tag{C14}$$

APPENDIX D: FULL EXAMPLE SIMULATIONS

We show all variables for the example simulations in Sec. IV A, i.e., for $T = 225$ K, $p = 300$ hPa, $F = 1$, in Figs. 11, 12, and 13.

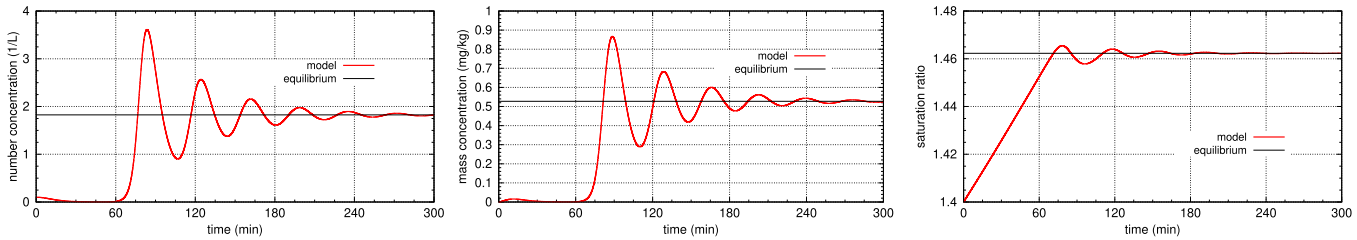

FIG. 11. Examples of solutions for $w = 0.01\ \mathrm{m\,s^{-1}}$ at $T = 225$ K, $p = 300$ hPa, and $F = 1$. Left: number concentration, middle: mass concentration, right: saturation ratio, red line; black lines indicate the equilibrium values.

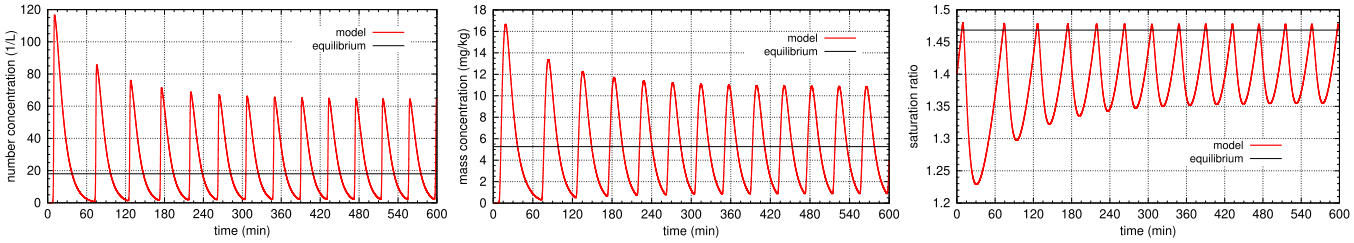

FIG. 12. Examples of solutions for $w = 0.10\,\mathrm{m\,s^{-1}}$ at $T = 225\,\mathrm{K}$, $p = 300\,\mathrm{hPa}$, and $F = 1$. Left: number concentration, middle: mass concentration, right: saturation ratio, red line; black lines indicate the equilibrium values.

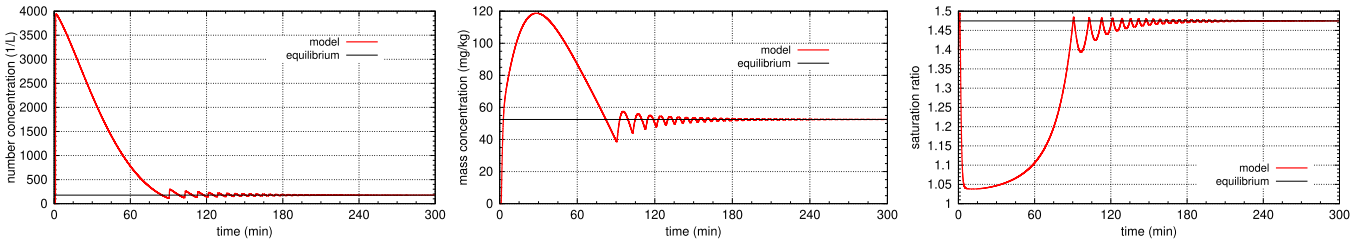

FIG. 13. Examples of solutions for $w = 1.00\,\mathrm{m\,s^{-1}}$ at $T = 225\,\mathrm{K}$, $p = 300\,\mathrm{hPa}$, and $F = 1$. Left: number concentration, middle: mass concentration, right: saturation ratio, red line; black lines indicate the equilibrium values.

REFERENCES

[1] C. J. Stubenrauch, A. G. Feofilov, S. E. Protopapadaki, and R. Armante, "Cloud climatologies from the infrared sounders AIRS and IASI: Strengths and applications," Atmos. Chem. Phys. **17**, 13625–13644 (2017).

[2] P. Gallo, K. Amann-Winkel, C. A. Angell, M. A. Anisimov, F. Caupin, C. Chakravarty, E. Lascaris, T. Loerting, A. Z. Panagiotopoulos, J. Russo, J. A. Sellberg, H. E. Stanley, H. Tanaka, C. Vega, L. Xu, and L. G. M. Pettersson, "Water: A tale of two liquids," Chem. Rev. **116**, 7463–7500 (2016).

[3] P. Gallo, T. Loerting, and F. Sciortino, "Supercooled water: A polymorphic liquid with a cornucopia of behaviors," J. Chem. Phys. **151**, 210401 (2019).

[4] Y. Zhang, A. Macke, and F. Albers, "Effect of crystal size spectrum and crystal shape on stratiform cirrus radiative forcing," Atmos. Res. **52**, 59–75 (1999).

[5] T. Chen, W. Rossow, and Y. Zhang, "Radiative effects of cloud-type variations," J. Clim. **13**, 264–286 (2000).

[6] M. Krämer, C. Rolf, N. Spelten, A. Afchine, D. Fahey, E. Jensen, S. Khaykin, T. Kuhn, P. Lawson, A. Lykov, L. L. Pan, M. Riese, F. Stroh, T. Thornberry, V. Wolf, S. Woods, P. Spichtinger, J. Quaas, and O. Sourdeval, "A microphysics guide to cirrus—Part II: Climatologies of clouds and humidity from observations," Atmos. Chem. Phys. Discuss. **20**, 12569–12608 (2020).

[7] Q. Fu and K. Liou, "Parameterization of the radiative properties of cirrus clouds," J. Atmos. Sci. **50**, 2008–2025 (1993).

[8] M. Krämer, C. Rolf, A. Luebke, A. Afchine, N. Spelten, A. Costa, J. Meyer, M. Zoeger, J. Smith, R. L. Herman, B. Buchholz, V. Ebert, D. Baumgardner, S. Borrmann, M. Klingebiel, and L. Avallone, "A microphysics guide to cirrus clouds—Part 1: Cirrus types," Atmos. Chem. Phys. **16**, 3463–3483 (2016).

[9] H. Wernli, M. Boettcher, H. Joos, A. K. Miltenberger, and P. Spichtinger, "A trajectory-based classification of era-interim ice clouds in the region of the north atlantic storm track," Geophys. Res. Lett. **43**, 6657–6664, https://doi.org/10.1002/2016GL068922 (2016).

[10] V. I. Khvorostyanov, "Mesoscale processes of cloud formation, cloud-radiation interaction, and their modelling with explicit cloud microphysics," Atmos. Res. **39**, 1–67 (1995).

[11] A. P. Khain, K. D. Beheng, A. Heymsfield, A. Korolev, S. O. Krichak, Z. Levin, M. Pinsky, V. Phillips, T. Prabhakaran, A. Teller, S. C. van den Heever, and J. I. Yano, "Representation of microphysical processes in cloud-resolving models: Spectral (bin) microphysics versus bulk parameterization," Rev. Geophys. **53**, 247–322, https://doi.org/10.1002/2014RG000468 (2015).

[12] T. Hauf, "Microphysical kinetics in phase space: The warm rain process," Atmos. Res. **29**, 55–84 (1993).

[13] U. Wacker, "Structural stability in cloud physics using parameterized microphysics," Beitr. Phys. Atmosph. **65**, 231–242 (1992).

[14] U. Wacker, "Competition of precipitation particles in a model with parameterized cloud particles," J. Atmos. Sci. **52**, 2577–2589 (1995).

[15] U. Wacker, "Nonlinear effects in a conceptual multilayer cloud model," Nonlinear Process. Geophys. **13**, 99–107 (2006).

[16] I. Koren and G. Feingold, "Aerosol–cloud–precipitation system as a predator-prey problem," Proc. Natl. Acad. Sci. U.S.A. **108**, 12227–12232 (2011).

[17] G. Feingold and I. Koren, "A model of coupled oscillators applied to the aerosol–cloud–precipitation system," Nonlinear Process. Geophys. **20**, 1011–1021 (2013).

[18] E. J. Spreitzer, M. P. Marschalik, and P. Spichtinger, "Subvisible cirrus clouds—A dynamical system approach," Nonlinear Process. Geophys. **24**, 307–328 (2017).

[19] W. Walter, *Ordinary Differential Equations*, Graduate Texts in Mathematics Vol. 182 (Springer Science & Business Media, 1998), pp. XI,384.

[20] M. Hanke and N. Porz, "Unique solvability of a system of ordinary differential equations modeling a warm cloud parcel," SIAM J. Appl. Math. **80**, 706–724 (2020).

[21] T. Koop, B. Luo, A. Tsias, and T. Peter, "Water activity as the determinant for homogeneous ice nucleation in aqueous solutions," Nature **406**, 611–614 (2000).

[22] P. Spichtinger, P. Marschalik, and M. Baumgartner, "Impact of formulations of the homogeneous nucleation rate on ice nucleation events in cirrus," Atmos. Chem. Phys. **23**, 2035–2060 (2023).

[23] D. Kondepudi and I. Prigogine, *Modern Thermodynamics: From Heat Engines to Dissipative Structures*, 2nd ed. (John Wiley & Sons, 2014), p. 560.

[24] D. M. Murphy and T. Koop, "Review of the vapour pressure of ice and supercooled water for atmospheric applications," Q. J. R. Meterorol. Soc. **131**, 1539–1565 (2005).

[25]J. Rosemeier, M. Baumgartner, and P. Spichtinger, "Intercomparison of warm-rain bulk microphysics schemes using asymptotics," Math. Clim. Weather Forecast. **4**, 104–124 (2018).
[26]K. G. Libbrecht, "The physics of snow crystals," Rep. Prog. Phys. **68**, 855 (2005).
[27]M. P. Bailey and J. Hallett, "A comprehensive habit diagram for atmospheric ice crystals: Confirmation from the laboratory, AIRS II, and other field studies," J. Atmos. Sci. **66**, 2888–2899 (2009).
[28]L. Grulich, R. Weigel, A. Hildebrandt, M. Wand, and P. Spichtinger, "Automatic shape detection of ice crystals," J. Comput. Sci. **54**, 101429 (2021).
[29]M. Baumgartner and P. Spichtinger, "Local interactions by diffusion between mixed-phase hydrometeors: Insights from model simulations," Math. Clim. Weather Forecast. **3**, 64 (2017).
[30]A. Heymsfield and J. Iaquinta, "Cirrus crystal terminal velocities," J. Atmos. Sci. **57**, 916–938 (2000).
[31]P. Spichtinger and K. M. Gierens, "Modelling of cirrus clouds—Part 1A: Model description and validation," Atmos. Chem. Phys. **9**, 685–706 (2009).
[32]F. Schröder, B. Kärcher, C. Duroure, J. Ström, A. Petzold, J.-F. Gayet, B. Strauss, P. Wendling, and S. Borrmann, "On the transition of contrails into cirrus clouds," J. Atmos. Sci. **57**, 464–480 (2000).
[33]H. Köhler, "The nucleus in and the growth of hygroscopic droplets," Trans. Faraday Soc. **32**, 1152–1161 (1936).
[34]M. Baumgartner and P. Spichtinger, "Diffusional growth of cloud particles: Existence and uniqueness of solutions," Theor. Comput. Fluid Dyn. **32**, 47–62 (2018).
[35]D. Lamb and J. Verlinde, *Physics and Chemistry of Clouds* (Cambridge University Press, 2011).
[36]W. Hall and H. Pruppacher, "Survival of ice particles falling from cirrus clouds in subsaturated air," J. Atmos. Sci. **33**, 1995–2006 (1976).
[37]J. Dixon, *The Shock Absorber Handbook* (Wiley, 2007), p. 432.
[38]K. Gierens and S. Bretl, "Analytical treatment of ice sublimation and test of sublimation parameterisations in two-moment ice microphysics models," Atmos. Chem. Phys. **9**, 7481–7490 (2009).
[39]H. R. Pruppacher and J. D. Klett, *Microphysics of Clouds and Precipitation*, Atmospheric and Oceanographic Sciences Library Vol. 18 (Kluwer Academic Publishers, Dordrecht, 2010).
[40]P. Spichtinger and D. J. Cziczo, "Impact of heterogeneous ice nuclei on homogeneous freezing events in cirrus clouds," J. Geophys. Res. **115**, D14208, https://doi.org/10.1029/2009jd012168 (2010).
[41]J. E. Kay, M. Baker, and D. Hegg, "Microphysical and dynamical controls on cirrus cloud optical depth distributions," J. Geophys. Res. **111**, D24205, https://doi.org/10.1029/2005JD006916 (2006).
[42]M. Kajikawa and A. Heymsfield, "Aggregation of ice crystals in cirrus," J. Atmos. Sci. **46**, 3108–3121 (1989).
[43]E. Kienast-Sjögren, P. Spichtinger, and K. Gierens, "Formulation and test of an ice aggregation scheme for two-moment bulk microphysics schemes," Atmos. Chem. Phys. **13**, 9021–9037 (2013).
[44]C. R. Harris, K. J. Millman, S. J. van der Walt, R. Gommers, P. Virtanen, D. Cournapeau, E. Wieser, J. Taylor, S. Berg, N. J. Smith, R. Kern, M. Picus, S. Hoyer, M. H. van Kerkwijk, M. Brett, A. Haldane, J. F. del Río, M. Wiebe, P. Peterson, P. Gérard-Marchant, K. Sheppard, T. Reddy, W. Weckesser, H. Abbasi, C. Gohlke, and T. E. Oliphant, "Array programming with NumPy," Nature **585**, 357–362 (2020).
[45]Y. A. Kuznetsov, *Elements of Applied Bifurcation Theory*, 2nd ed., Applied Mathematical Sciences Vol. 112 (Springer-Verlag, New York, 1998), p. xx+591.
[46]M. Golubitsky and D. G. Schaeffer, *Singularities and Groups in Bifurcation Theory* (Springer, New York, 1985).
[47]J. Guckenheimer and P. Holmes, *Nonlinear Oscillations, Dynamical Systems, and Bifurcations of Vector Fields*, 7th ed., Applied Mathematical Sciences No. 42 (Springer, New York, 2002), p. XVI, 462.
[48]P. Spichtinger and M. Krämer, "Tropical tropopause ice clouds: A dynamic approach to the mystery of low crystal numbers," Atmos. Chem. Phys. **13**, 9801–9818 (2013).
[49]G. Pruessner, *Self-Organised Criticality: Theory, Models and Characterisation* (Cambridge University Press, 2012).
[50]B. Kärcher and U. Lohmann, "A parameterization of cirrus cloud formation: Homogeneous freezing of supercooled aerosols," J. Geophys. Res.: Atmos. **107**, AAC 4-1–AAC 4-10, https://doi.org/10.1029/2001JD000470 (2002).
[51]H. Joos, P. Spichtinger, and U. Lohmann, "Orographic cirrus in a future climate," Atmos. Chem. Phys. **9**, 7825–7845 (2009).
[52]H. Joos, P. Spichtinger, P. Reutter, and F. Fusina, "Influence of heterogeneous freezing on the microphysical and radiative properties of orographic cirrus clouds," Atmos. Chem. Phys. **14**, 6835–6852 (2014).
[53]J. Rosemeier and P. Spichtinger, "Pattern formation in clouds via turing instabilities," Math. Clim. Weather Forecast. **6**, 75–96 (2020).
[54]A. Turing, "The chemical basis of morphogenesis," Philos. Trans. R. Soc., B **237**, 37–72 (1952).
[55]M. Krämer, C. Rolf, and N. Spelten (2020). "The Cirrus Guide II In-situ Aircraft," FZ-Juelich B2SHARE. https://doi.org/10.34730/266ca2a41f4946ff97d874bfa458254c